Geoneutrino observation with KamLAND

Research Center for Neutrino Science, Tohoku University, Japan
Nanami Kawada

Neutrino Geoscience 2025, Kingston, Canada

Contents

- The KamLAND experiment
- Result of geoneutrino observation
- Machine-learning powered event selection
- Construction of new detector

Contents

- The KamLAND experiment
- Result of geoneutrino observation
- Machine-learning powered event selection
- Construction of new detector

The KamLAND collaboration !!

TOHOKU UNIVERSITY

東京大学 THE UNIVERSITY OF TOKYO

大阪大学 OSAKA UNIVERSITY

Nikhef

TOKUSHIMA UNIVERSITY

VIRGINIA TECH

UNIVERSITY of HAWAI'I

THE UNIVERSITY OF TENNESSEE KNOXVILLE

MIT

BERKELEY LAB

TUNL

BU BOSTON UNIVERSITY

>50 researchers from US, Netherland and Japan

The KamLAND detector

Detector site and components

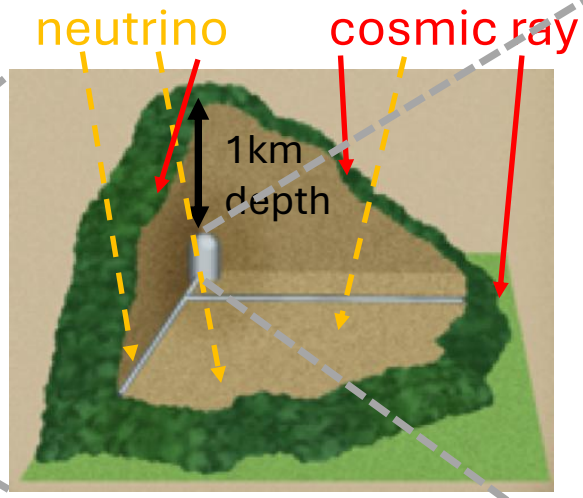

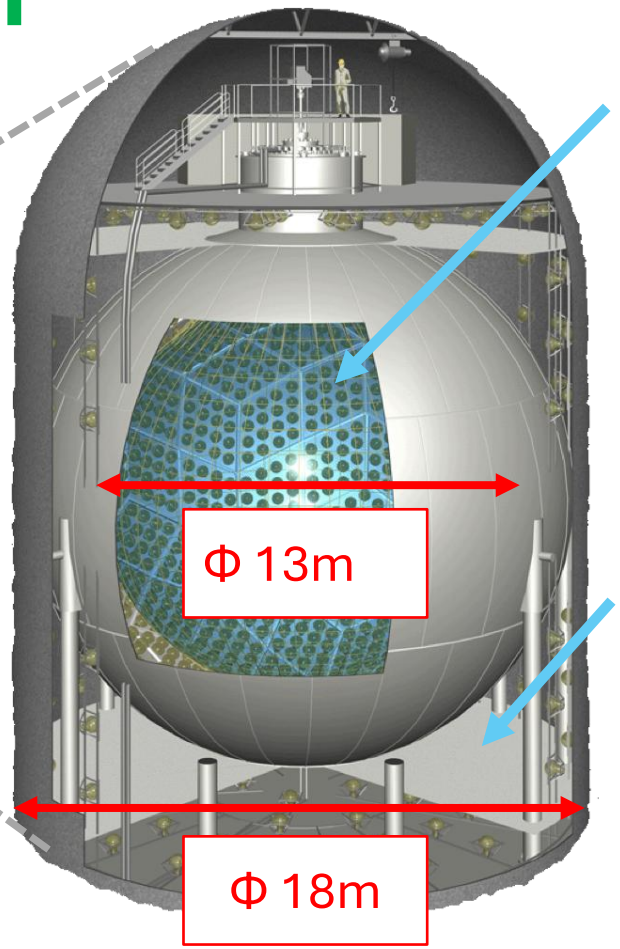

Scintillation inner detector

1kt purified liquid scintillator
(PC+Dodecane+PPO mixture)
1325 17” + 554 20” PMTs
photo coverage 34%
Neutrino detection

Water-cherenkov outer detector

3.2 kt purified water
225(140) 20” PMTs
passive shielding
active veto to muon

Neutrino detection channel

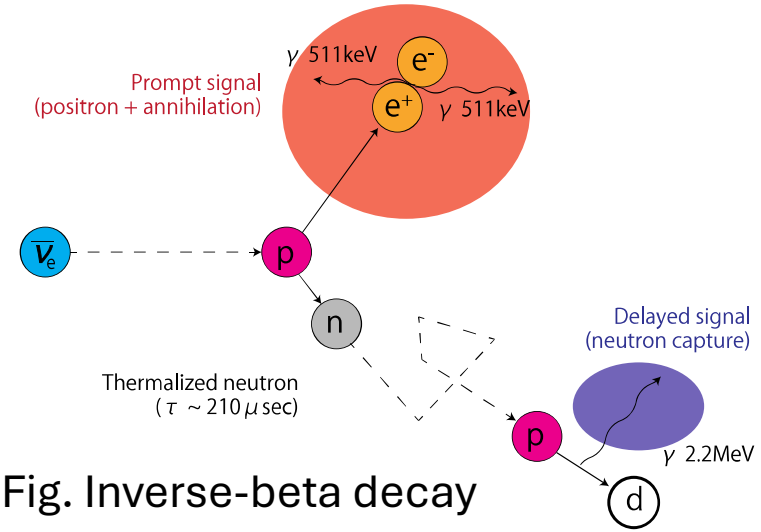

Fig. Inverse-beta decay

Anti-electron neutrino detection by inverse-beta decay

- ✓ Significant background reduction by two-fold coincidence
- ✓ Neutrino energy reconstruction from prompt scintillation
- ✗ No directional information → reactor neutrinos are background

History of geoneutrino observation in KamLAND

2002 Beginning of KamLAND

2005 Nature 436, 499–503

2011 Nature Geoscience 4, 467–651

2022 Geophysical Research Letters Volume 49, Issue 16, e2022GL099566

First evidence of geoneutrino detection

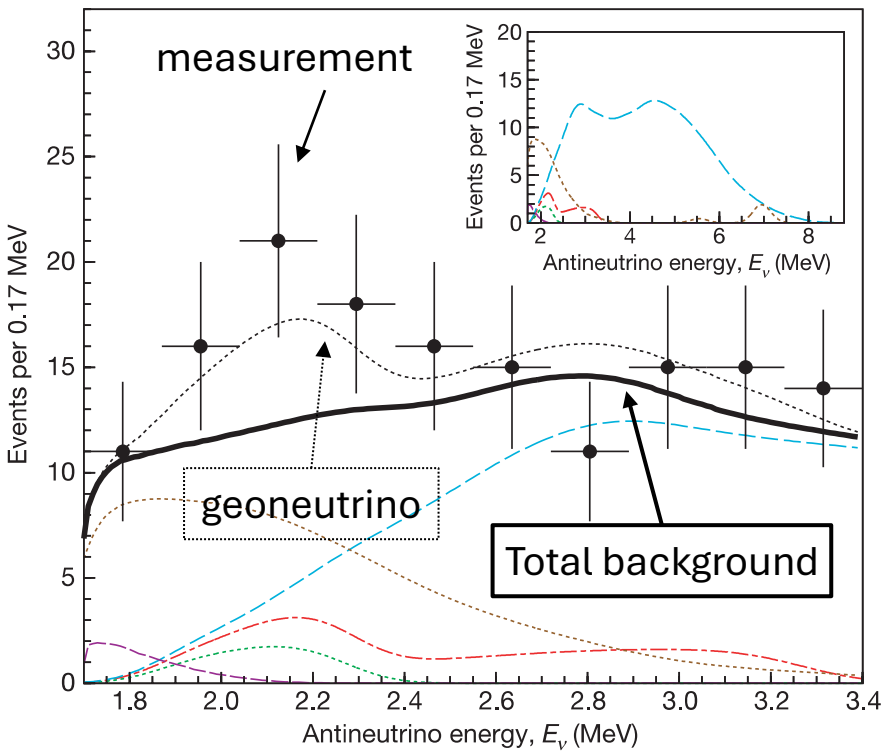

$28.0^{+15.6}_{-14.6}$ events (56% error)

749 days, 0.71×10^{32} proton-year

History of geoneutrino observation in KamLAND

2002 Beginning of KamLAND

2005 Nature 436, 499–503

2011 Nature Geoscience 4, 467–651

2022 Geophysical Research Letters Volume 49, Issue 16, e2022GL099566

First evidence of partial radiogenic Earth

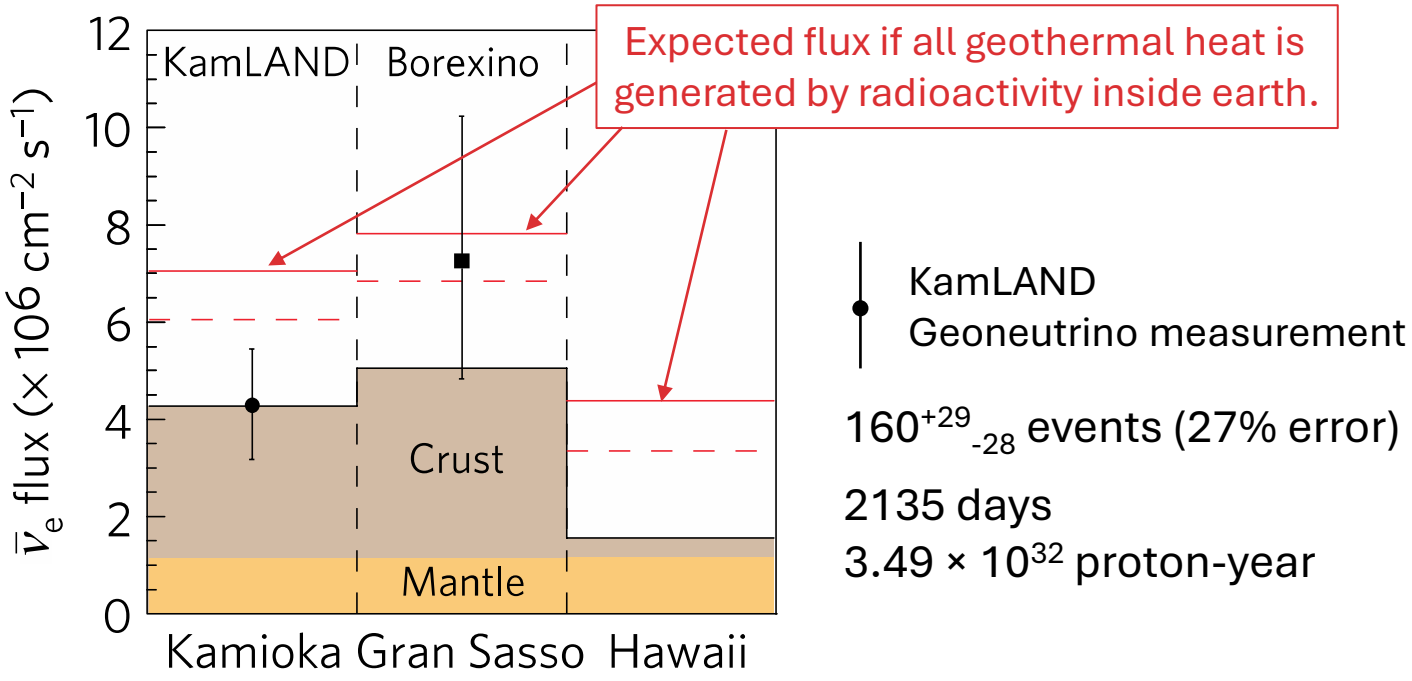

160^{+29}_{-28} events (27% error)

2135 days

3.49×10^{32} proton-year

This result implies radiogenic heat inside the Earth is fewer than total heat flow at the surface.

There is residual primordial heat is inside the Earth. Our planet is cooling.

History of geoneutrino observation in KamLAND

2002 Beginning of KamLAND

2005 Nature 436, 499–503

2011 Nature Geoscience 4, 467–651

2022 Geophysical Research Letters Volume 49, Issue 16, e2022GL099566

Reactor-off period in Japan

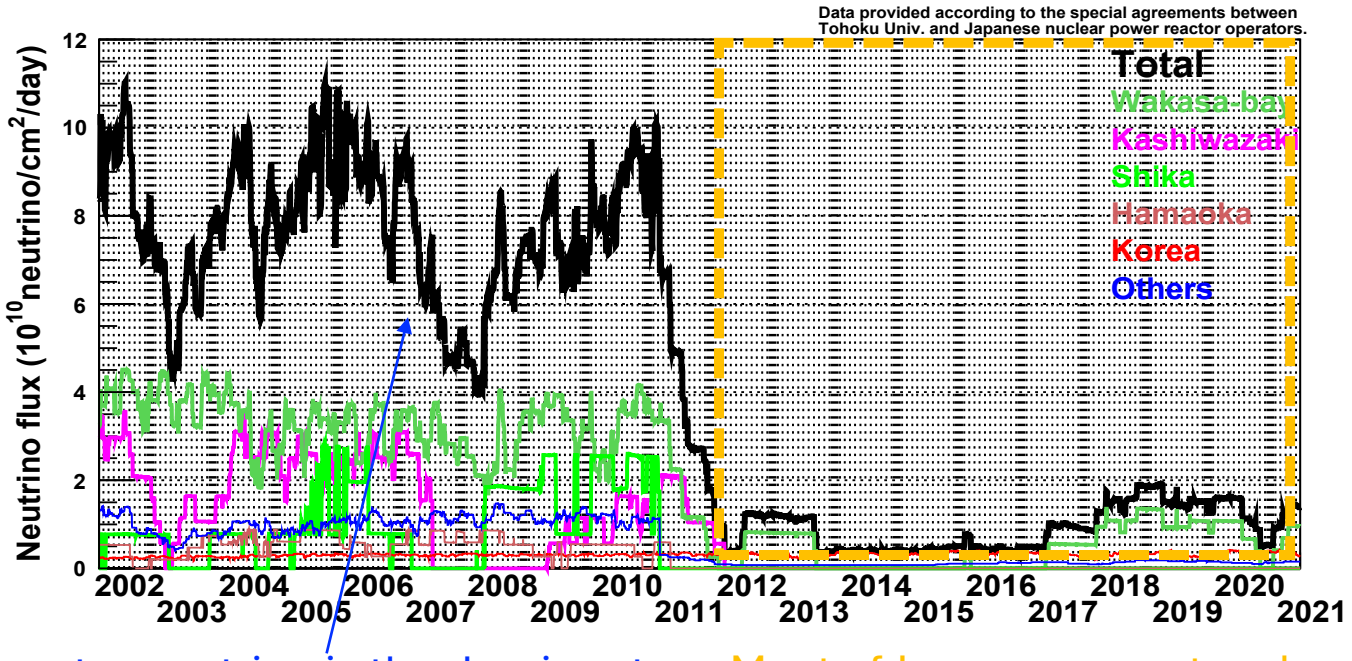

Reactor neutrino is the dominant background of geoneutrino signals.

Most of Japanese reactors have been shut down due to the 3.11 earthquake in 2011.

This "reactor-off" period gives us large signal-to-noise ratio of geoneutrino observation.

History of geoneutrino observation in KamLAND

2002 Beginning of KamLAND

2005 Nature 436, 499–503

2011 Nature Geoscience 4, 467–651

2022 Geophysical Research Letters Volume 49, Issue 16, e2022GL099566

First result of measurement in low-reactor period

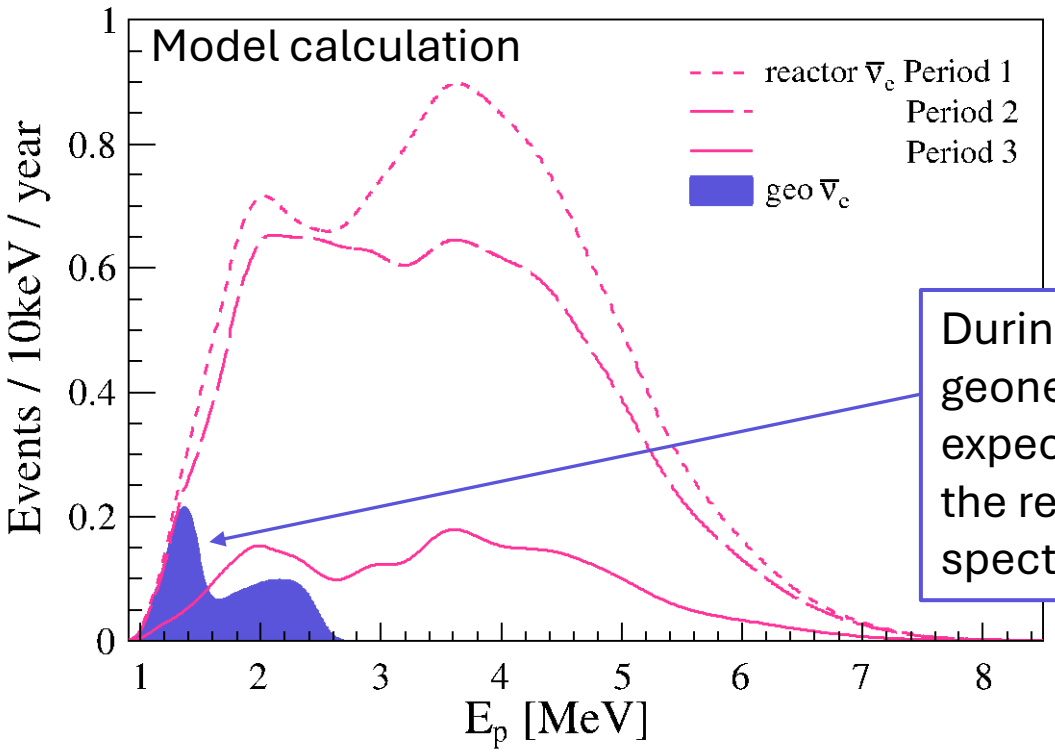

During low-reactor period, geoneutrino spectrum was expected to appear above the reactor neutrino spectrum.

Reactor off period significantly improved observation accuracy.

Contents

- The KamLAND experiment
- Result of geoneutrino observation
- Machine-learning powered event selection
- Construction of new detector

Best fit geoneutrino signals

Best-fit time variation

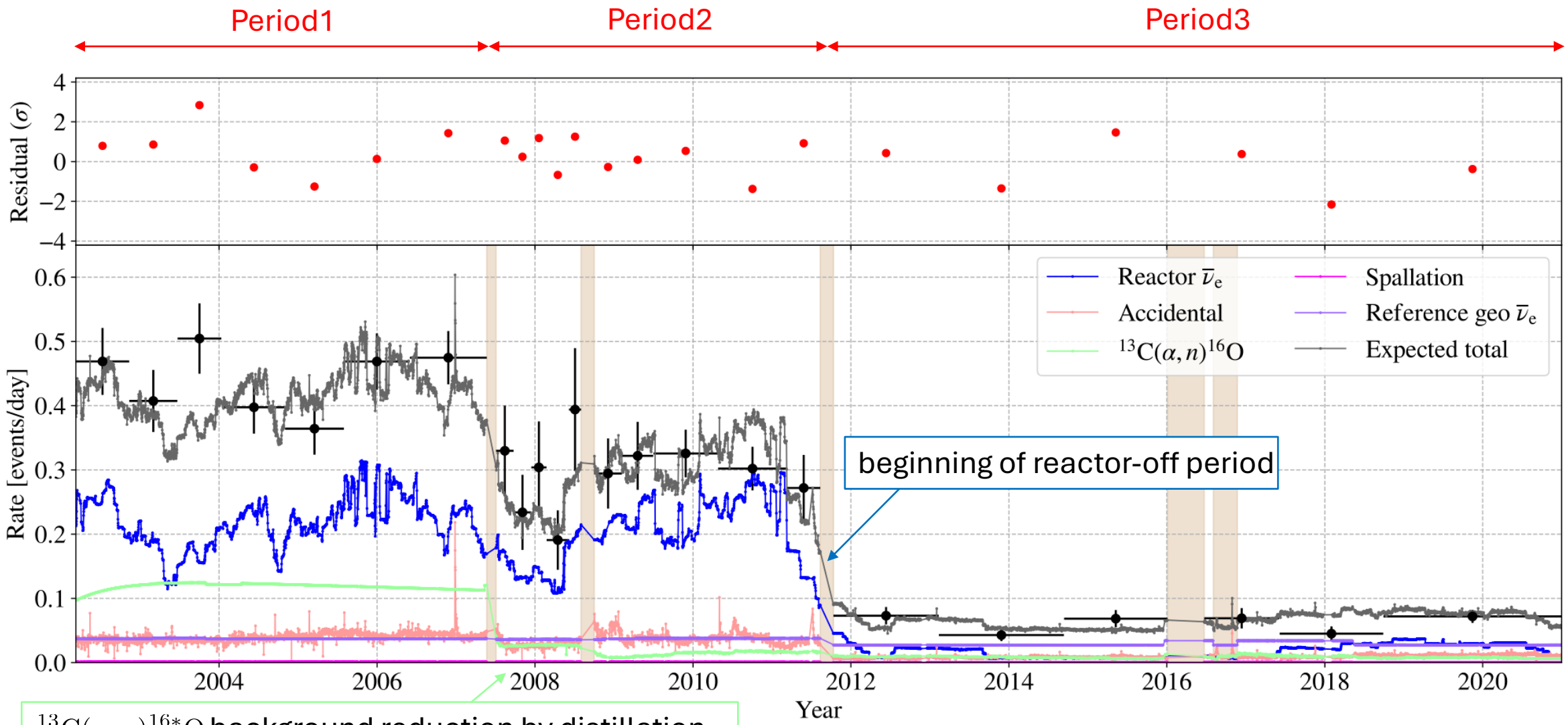

Best fit geoneutrino signals

Rate + Shape + Time un-binned Likelihood

Energy : 0.9 ≤ (Prompt Energy) ≤ 8.5 [MeV], 72 bins

Time : each KamLAND run (~24 hour bin)

scan parameter : geo $\overline{\nu}_e$ signal (U,Th)

fit parameter : $\Delta m_{21}{}^2, \theta_{12}, \theta_{13}$, backgrounds, systematics

Simultaneous scan of the oscillation parameters and geoneutrinos

Table. Best fit geoneutrino signals and backgrounds

	Period1	Period2	Period3	All Period
energy range [MeV]	0.9–2.6	0.9–2.6	0.9–2.6	0.9–2.6
live time [day]	1485.5	1151.5	2590.0	5227.0
Reactor $\overline{\nu}_e$	325.75	229.64	48.97	604.36
$^{13}C(\alpha,n)^{16}O$	177.66	20.42	22.18	222.26
Accidental	59.35	40.53	24.79	124.67
Spallation ($^8He/^9Li$)	1.52	1.05	1.69	4.26
Background total	620.21	334.07	171.98	1126.26
observed	651	363	164	1178

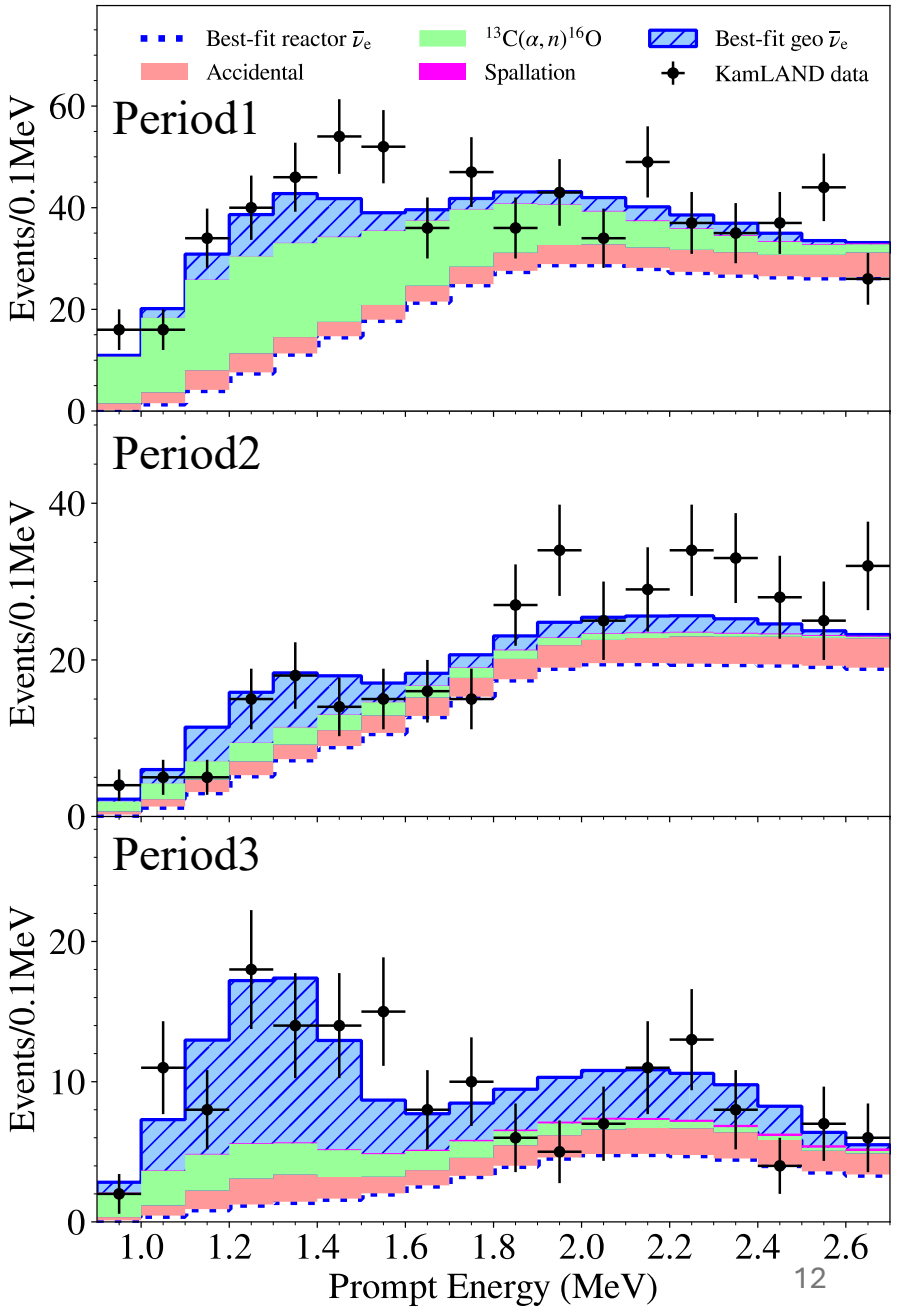

Geoneutrino flux measured by KamLAND

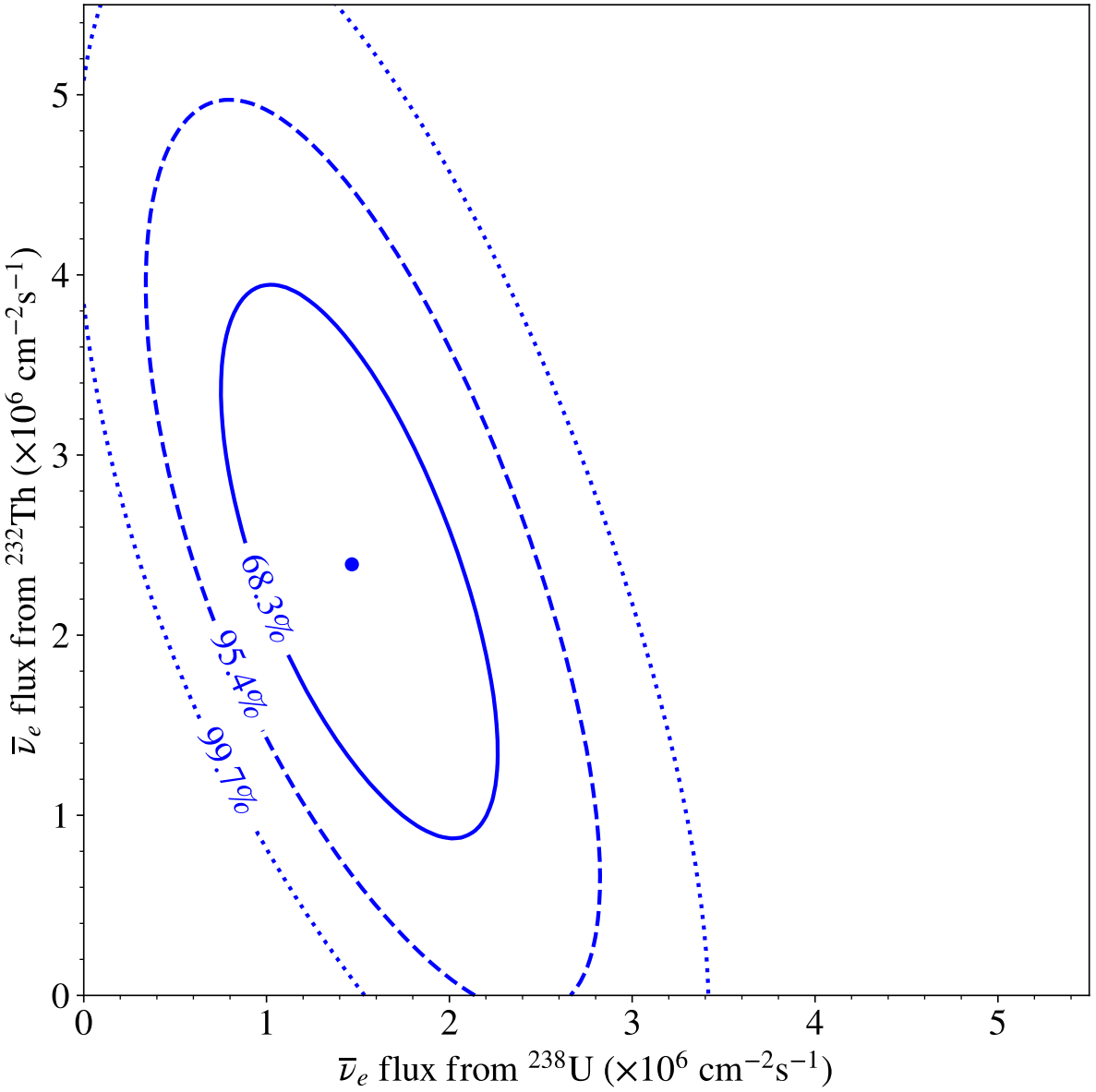

Best fit geoneutrino signals

	$N_{\mathrm{U/Th}}$ [event]	flux [$\times 10^5$ cm^{-2}s^{-1}]	flux [TNU]	0-signal rejection
U	$116.6^{+41.0}_{-38.5}$	$14.7^{+5.2}_{-4.8}$	$19.1^{+6.7}_{-6.3}$	3.343σ
Th	$57.5^{+24.5}_{-24.1}$	$23.9^{+10.2}_{-10.0}$	$9.7^{+4.1}_{-4.1}$	2.386σ
U + Th	$173.7^{+29.2}_{-27.7}$	$32.1^{+5.8}_{-5.3}$	$28.6^{+5.1}_{-4.8}$	8.3σ

KamLAND detected significant geoneutrino signal from both uranium and thorium inside the Earth.

Spectroscopic measurement of geoneutrinos from uranium and thorium was achieved.

Radiogenic heat measurement by KamLAND

KamLAND result

Crust estimation

central value : Enomoto 2007
uncertainty : Rudnick&Gao 2014
Th/U ratio : Wipperfurth et al 2018

Radiogenic heat from mantle

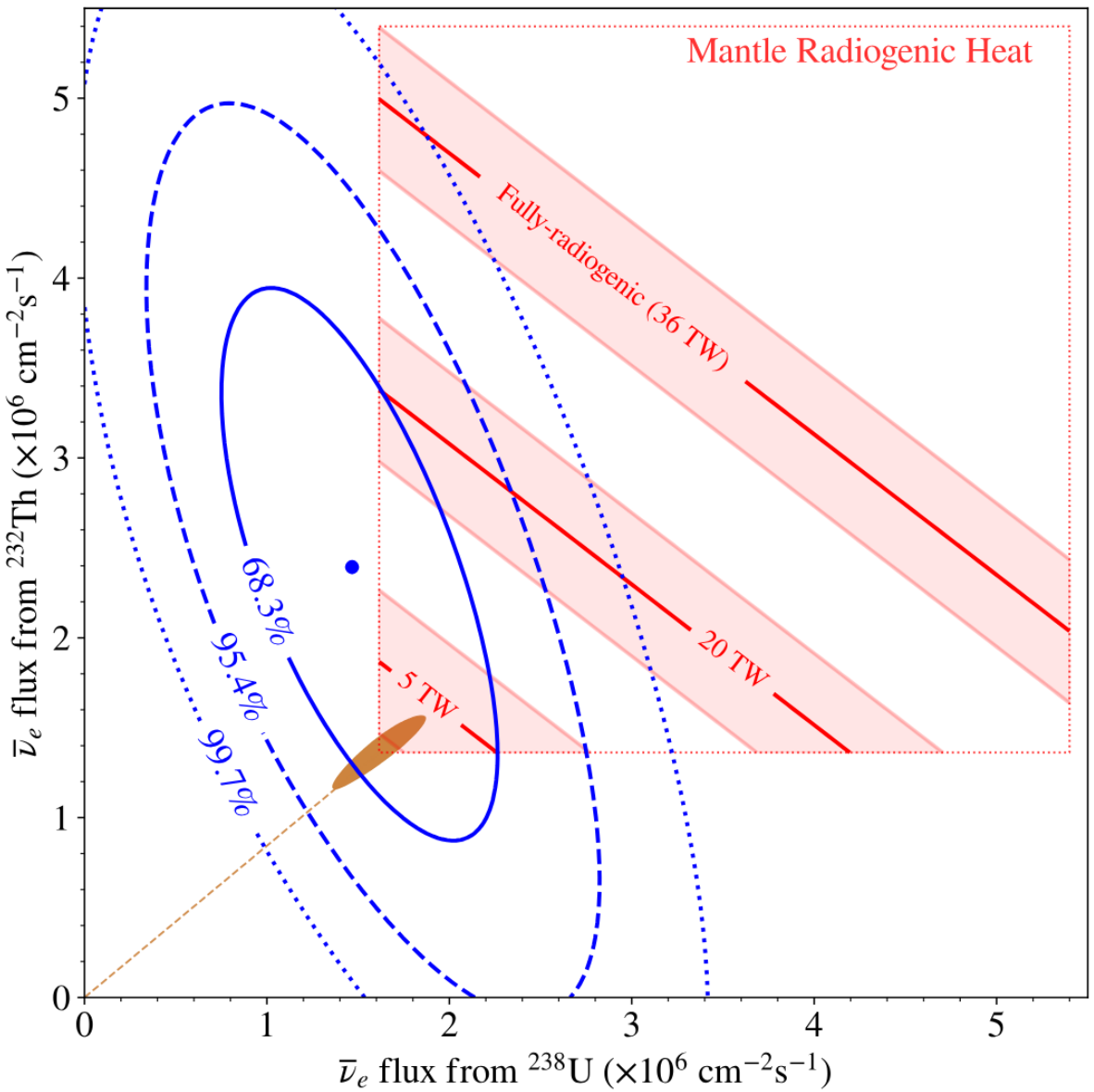

Conversion coefficients between flux and radiogenic heat in homogeneous mantle

$$Q^{\mathrm{U,Th}}_{\mathrm{mantle}} = (\Phi^{\mathrm{U,Th}} - \Phi^{\mathrm{U,Th}}_{\mathrm{crust}}) \frac{\mathrm{d}Q^{\mathrm{U,Th}}_{\mathrm{mantle}}}{\mathrm{d}\Phi^{\mathrm{U,Th}}_{\mathrm{mantle}}}$$

measured flux at the surface — flux estimate in crustal model

Adding heat estimate from crust,
^{238}U : 3.4 TW, ^{232}Th : 3.6 TW

$$Q^{\mathrm{U}} = 3.3^{+3.2}_{-0.8}\ \mathrm{TW}$$
$$Q^{\mathrm{Th}} = 12.1^{+8.3}_{-8.6}\ \mathrm{TW}$$
$$Q^{\mathrm{U}} + Q^{\mathrm{Th}} = 15.4^{+8.3}_{-7.9}\ \mathrm{TW}$$

Convective Uray ratio = $0.13^{+0.15}_{-0.06}$

Comparison to Earth models

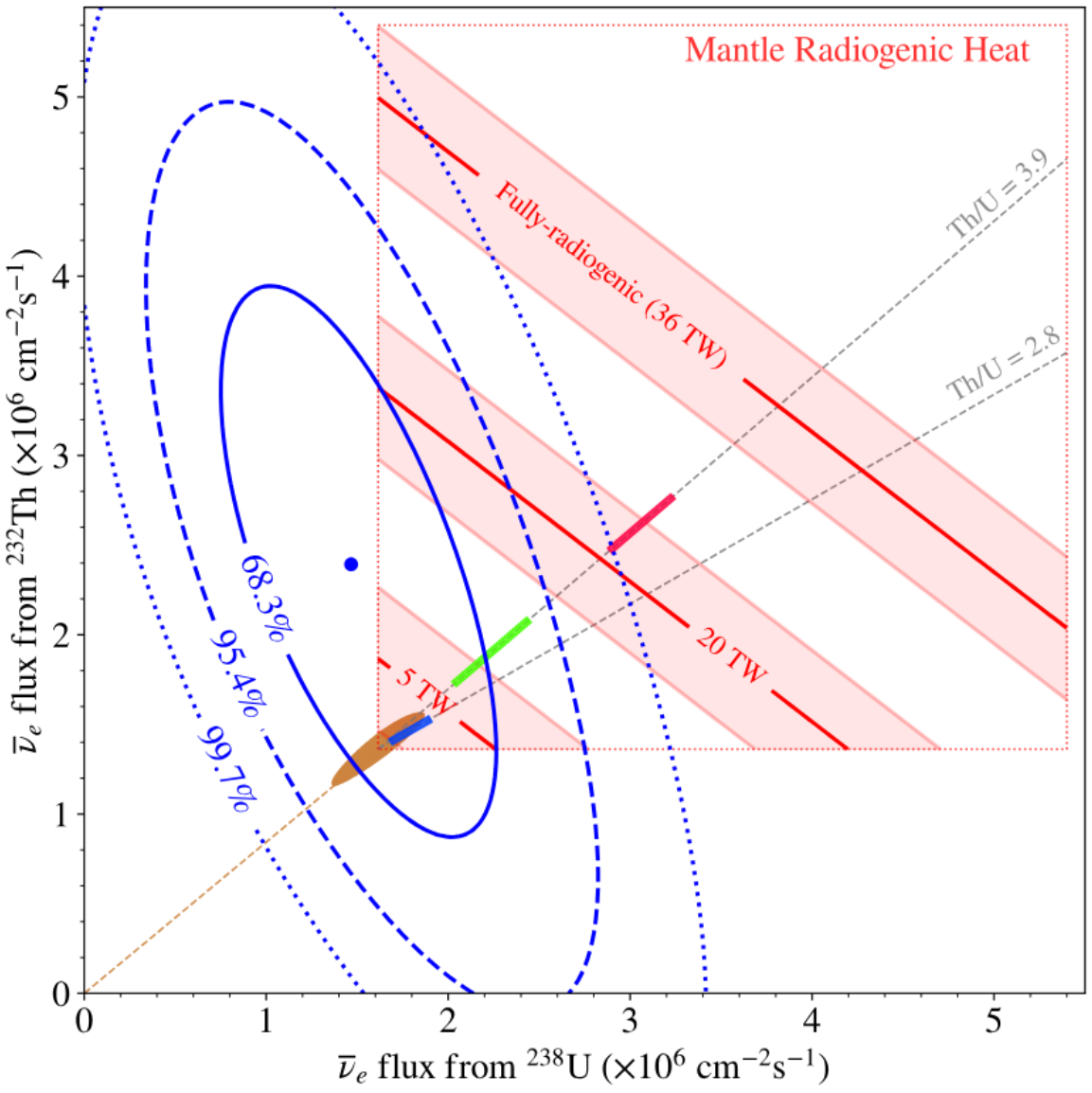

BSE models (Sramek et al 2013)

Low-Q (10-15 TW) Based on compositional analysis of enstatite chondrites and isotopic constraints (U : 12±2 ppb, Th : 43±4 ppb)

Middle-Q (17-22 TW) Based on compositional analysis of CI carbonaceous chondrites and earth samples (U : 20±4 ppb, Th : 80±13 ppb)

Consistent with the KamLAND data.

High-Q (>25 TW) Predicting relatively large amount of radiogenic heat for mantle convection. (U : 35±4 ppb, Th : 140±14 ppb)

Inconsistent with the KamLAND data

Contents

- The KamLAND experiment
- Result of geoneutrino observation
- Machine-learning powered event selection
- Construction of new detector

Toward improved precision in geoneutrino observation

Neutrino detection channel

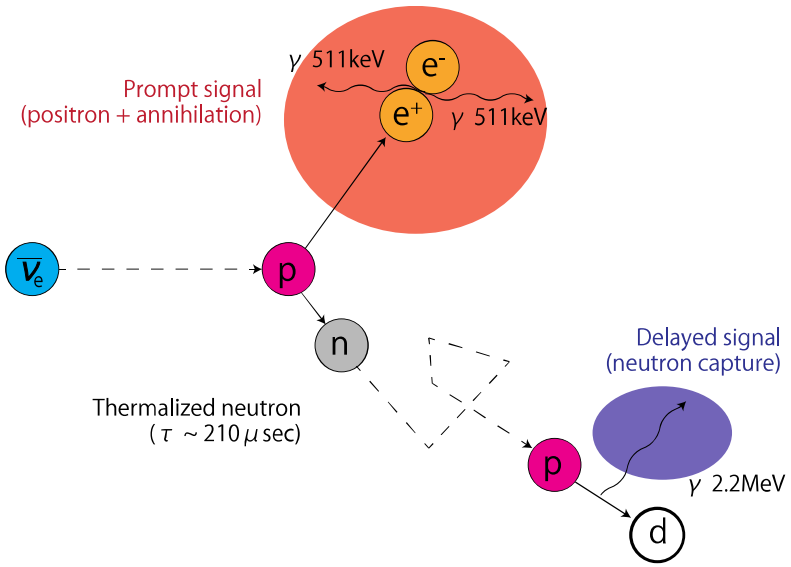

Anti-electron neutrinos induce inverse-beta decay(IBD), producing two temporally and spatially correlated signals. By applying delayed-coincidence selection, background events can be effectively suppressed.

IBD selection efficiency

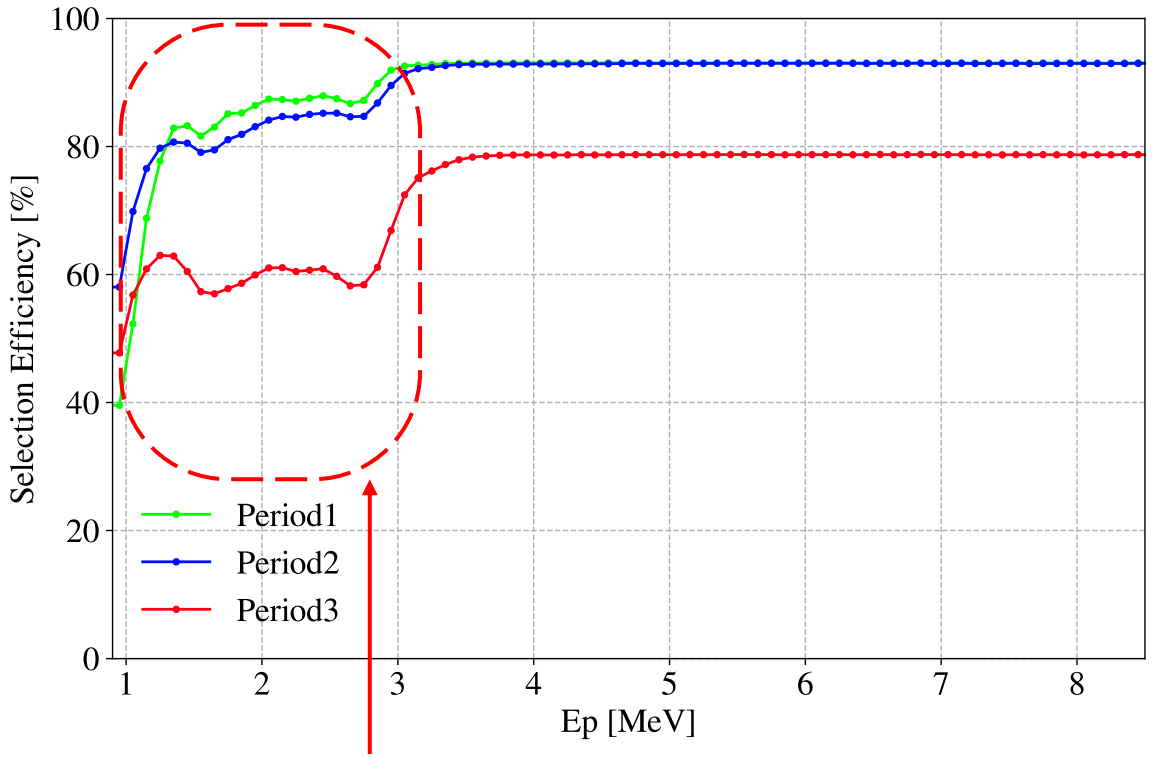

The selection efficiency of IBD signal is reduced due to accidental-coincidence background caused by external γ-ray from radioactive impurities.
There is room for improvement.

Conventional IBD selection

Box cut (1st layer)

Finding spacial and time coincident events with delayed-coincidence (DC)

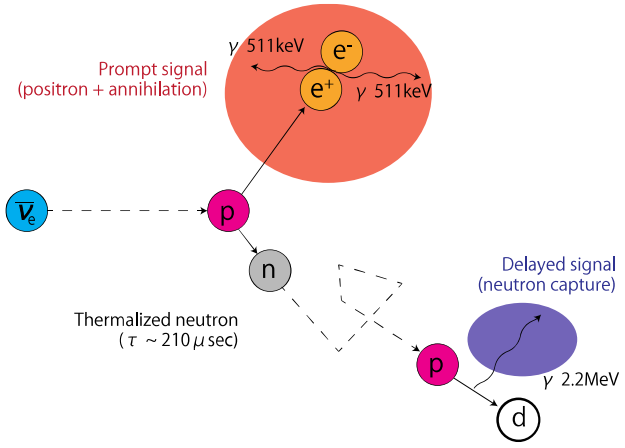

parameter	criteria
prompt energy [MeV]	$0.9 \leq E_{\mathrm{p}} < 8.5$
delayed energy [MeV]	$1.8 \leq E_{\mathrm{d}} < 2.6$ $4.4 \leq E_{\mathrm{d}} < 5.6$
space correlation [m]	$\Delta R < 2.0$
time correlation [μs]	$0.5 \leq \Delta T < 1000$
fiducial volume [m]	$R_{\mathrm{p}} < 6$ & $R_{\mathrm{d}} < 6$

LikelihoodRatio selection (2nd layer)

Probability density functions (PDFs) are constructed from DC parameters for both IBD signal and accidental background. A likelihood ratio derived from PDFs is used to classify each DC pair as an IBD signal or accidental background.

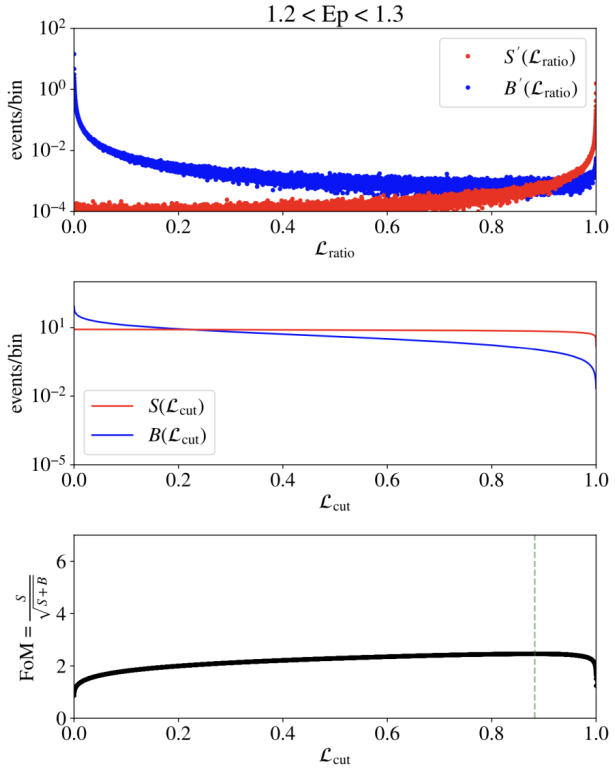

$$f_{\overline{\nu}_{\mathrm{e}}} = f_{\overline{\nu}_{\mathrm{e}}}(E_{\mathrm{p}}, E_{\mathrm{d}}, \Delta R, \Delta T, R_{\mathrm{p}}, R_{\mathrm{d}})$$

: Signal PDF (Geant4 simulation)

$$f_{\mathrm{accidental}} = f_{\mathrm{accidental}}(E_{\mathrm{p}}, E_{\mathrm{d}}, \Delta R, \Delta T, R_{\mathrm{p}}, R_{\mathrm{d}})$$

: Accidental PDF (data driven)

$$\mathcal{L}_{\mathrm{ratio}}(E_{\mathrm{p}}) = \frac{f_{\overline{\nu}_{\mathrm{e}}}}{f_{\overline{\nu}_{\mathrm{e}}} + f_{\mathrm{accidental}}}$$

: Likelihood ratio;
The probability that an DC pair is a IBD reaction

This approach does not account for inter-parameter correlations.
Figure-of-Merit loss arises from binning in PDF construction.

Conventional IBD selection

Box cut (1st layer)

Finding spacial and time coincident events with delayed-coincidence (DC)

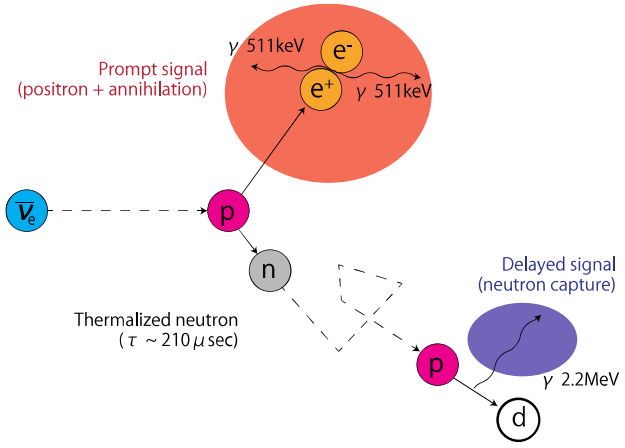

parameter	criteria
prompt energy [MeV]	$0.9 \leq E_p < 8.5$
delayed energy [MeV]	$1.8 \leq E_d < 2.6$ $4.4 \leq E_d < 5.6$
space correlation [m]	$\Delta R < 2.0$
time correlation [μs]	$0.5 \leq \Delta T < 1000$
fiducial volume [m]	$R_p < 6$ & $R_d < 6$

~~LikelihoodRatio selection (2nd layer)~~

Gradient Boosted Decision Tree selection (2nd layer)

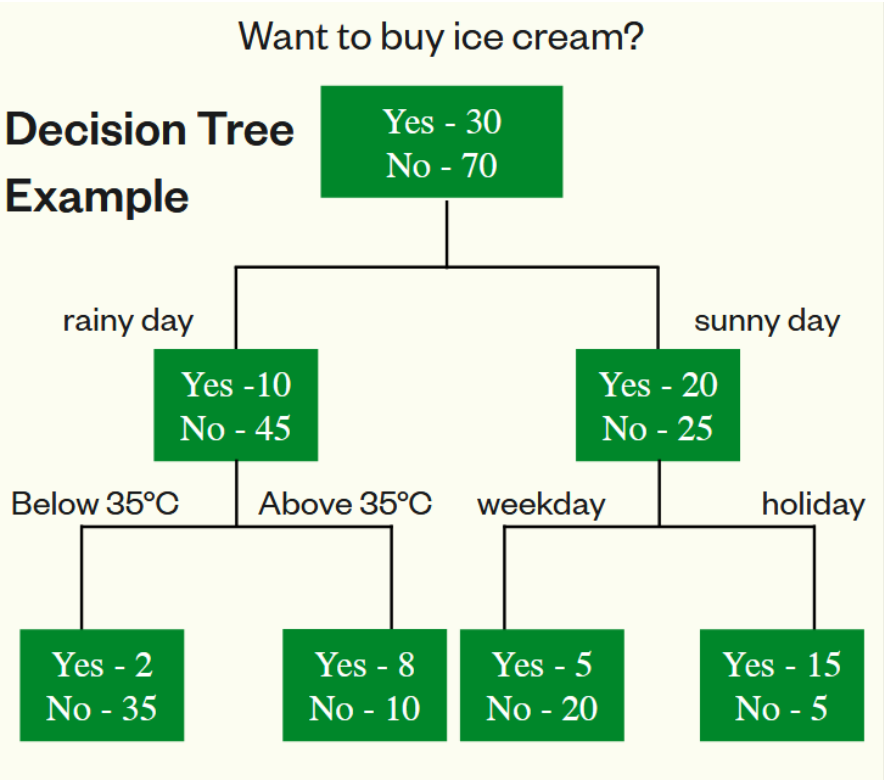

IBD selection with Gradient Boosted Decision Tree

Decision Tree

Machine-learning method effective for structured/tabular data.
Data split based on feature values, forming a tree-like structure.

Gradient Boosted Decision Tree

Ensemble method combining multiple decision tree to improve prediction accuracy. Each tree corrects errors from the previous one.

Training and validation

Training and validation use Geant4-simulated IBD and data-driven accidental background from time-shifted coincidence—same setup as conventional procedure; GBDT replaces the LikelihoodRatio function.

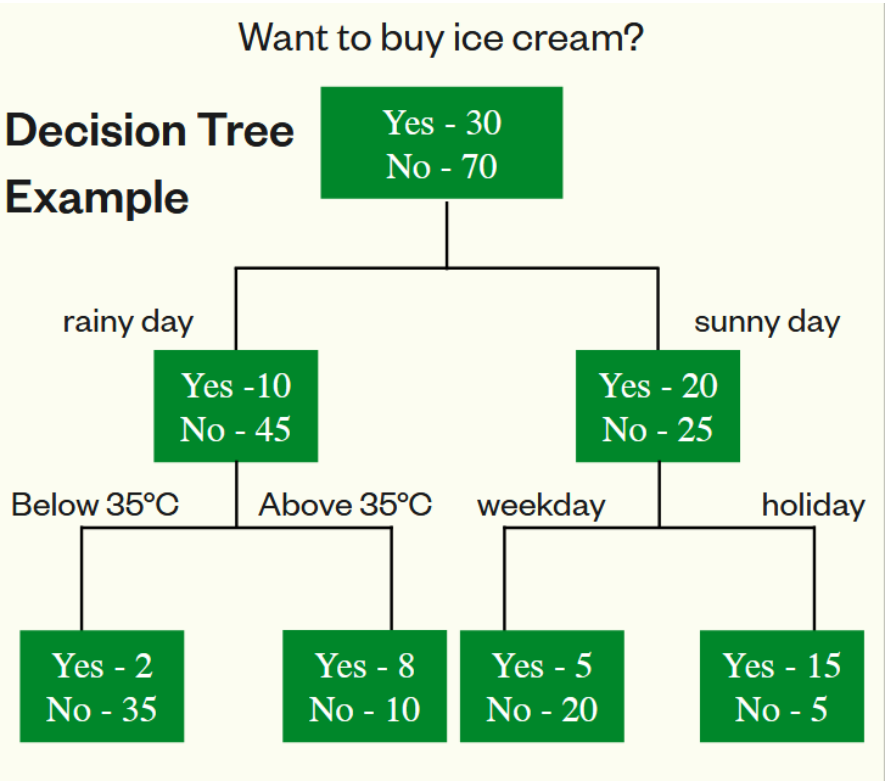

	Correlation between parameters	FoM loss by binning
Conventional LikelihoodRatio	× ignored	× binned
Gradient Boosted Decision Tree	✓ inherent	✓ avoided (unbinned)

Improvement in IBD selection efficiency

Conventional LikelihoodRatio selection

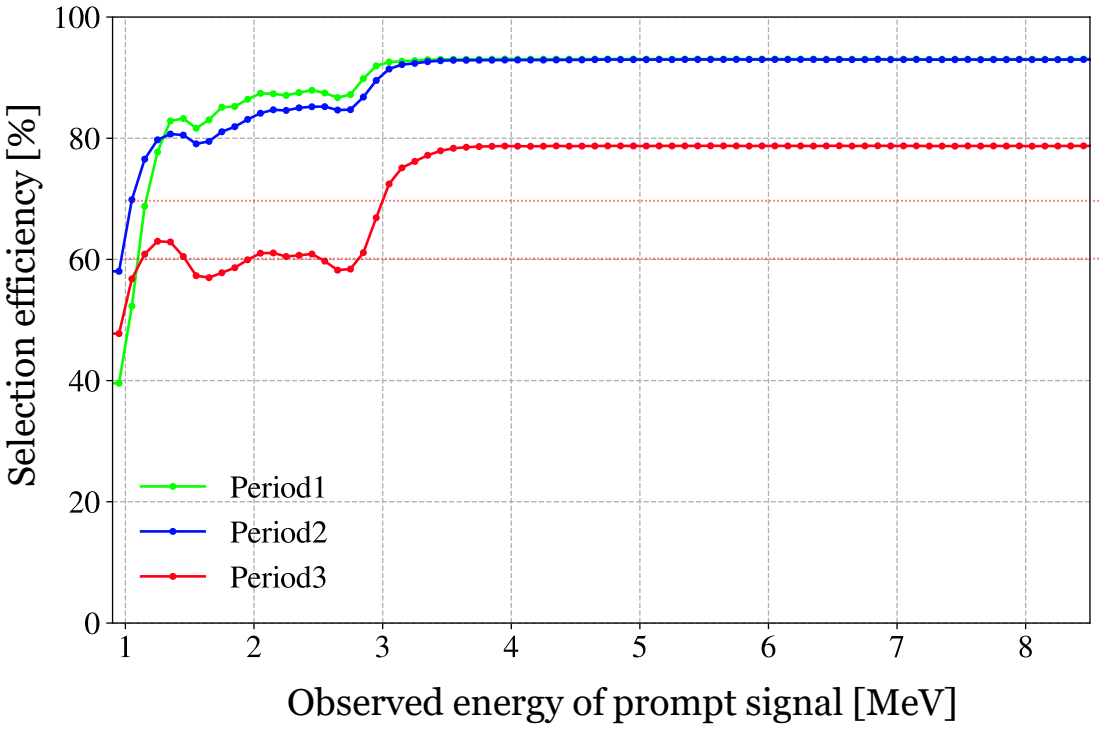

GBDT selection

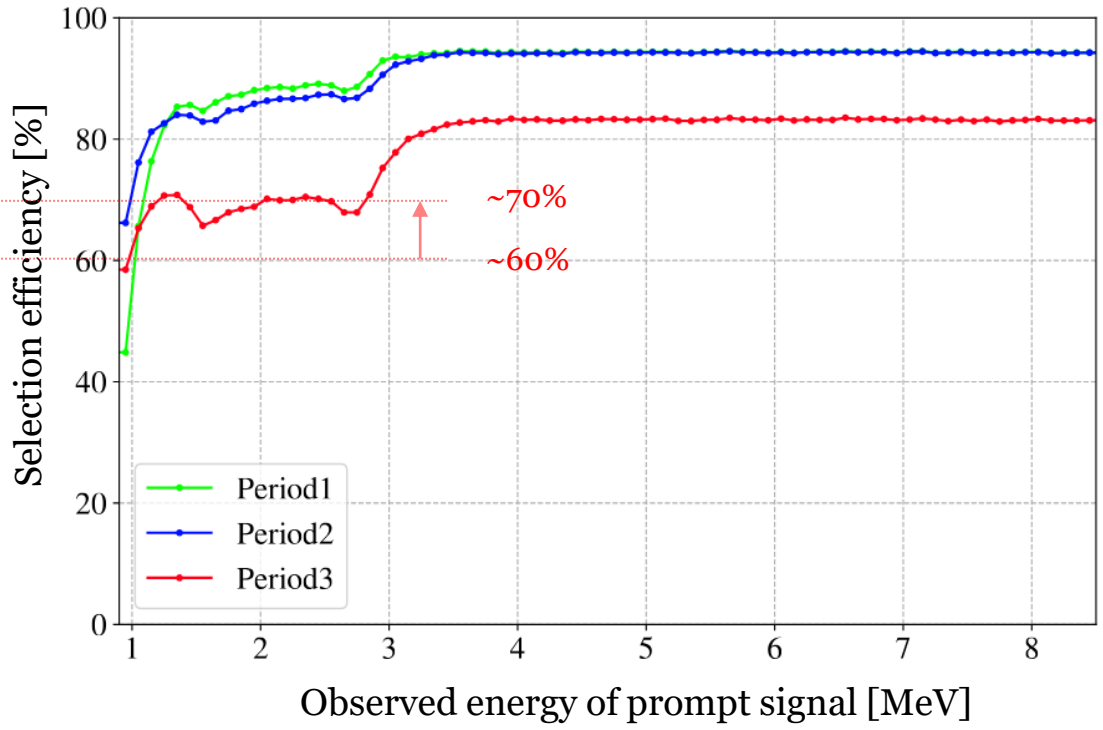

- **IBD selection efficiency in Period3 (low-reactor phase) was ~60% in the geoneutrino energy region (<3 MeV); introducing GBDT improved it to ~70%.**
- **Further gains are anticipated though complementary development including PID.**

Contents

- The KamLAND experiment
- Result of geoneutrino observation
- Machine-learning powered event selection
- Construction of new detector

KamLAND2(-Zen)

Frequently asked:
"KamLAND2" is new detector.
"KamLAND2-Zen" is next 0νββ search experiment using KamLAND2 not "KamLAND-Zen2".

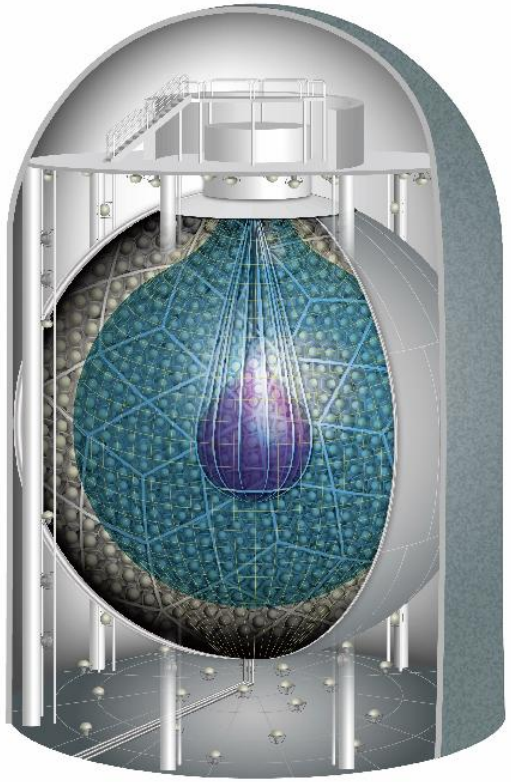

KamLAND2-Zen

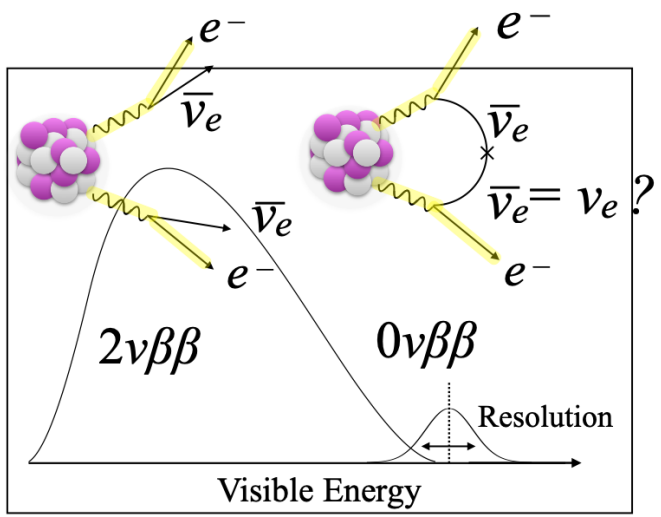

- KamLAND-Zen : Neutrinoless double-beta decay (0νββ) search using KamLAND.
- The isotope ^{136}Xe is installed at the center of the detector as the source of 0νββ.
- KamLAND-Zen 800 phase was completed in 2024.
- Construction of KamLAND2-Zen construction is currently underway to achieve further sensitivity to 0νββ.

While KamLAND2's primary target is neutrinoless double-beta decay, improved energy/vertex resolution is expected to enhance selection efficiency for antineutrino observation.

Detector status and prospect

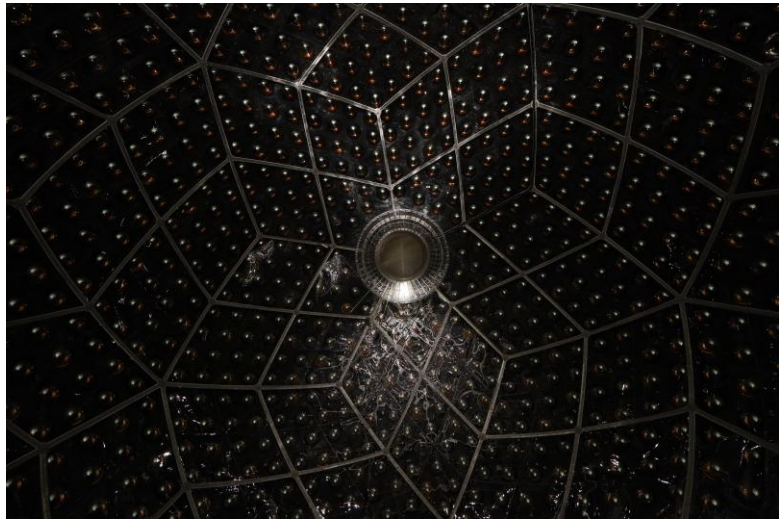

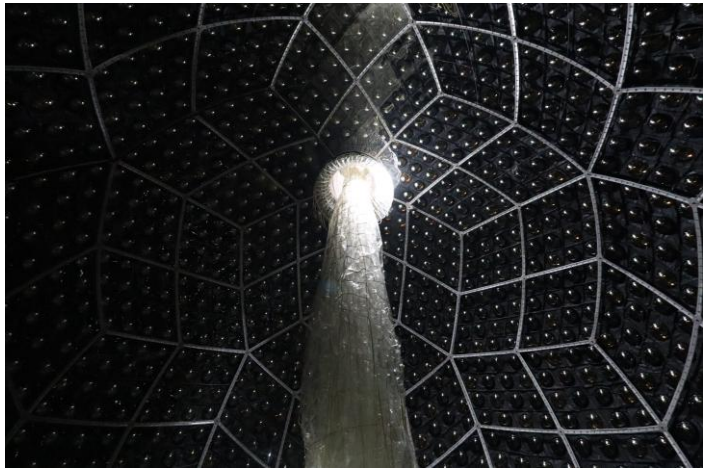

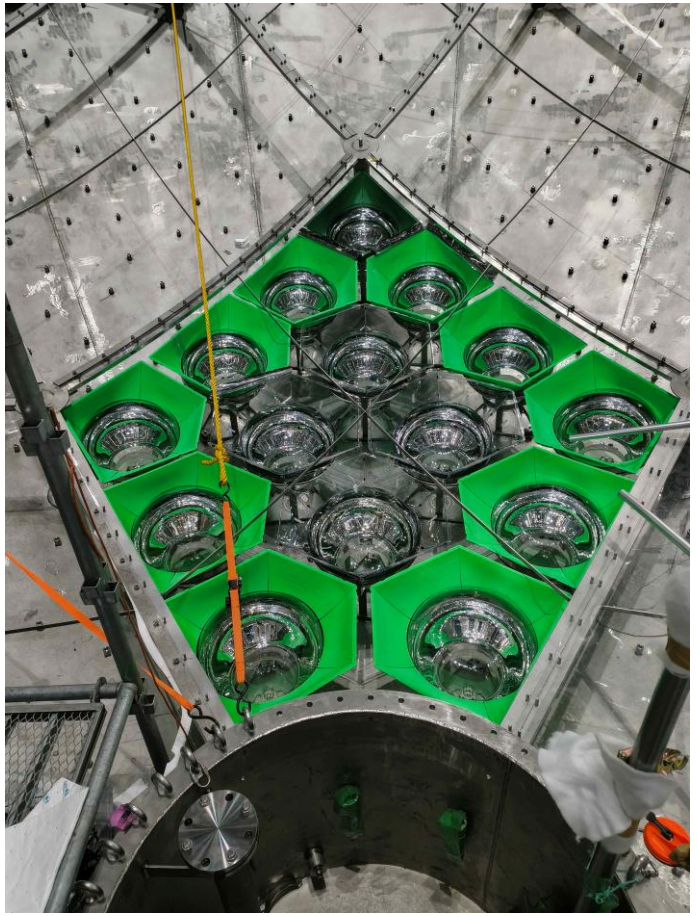

KamLAND completed data-taking in 2024 and is now under upgrade work.
R&D on new LS, light-collecting mirrors, balloon and DAQ is underway.
KamLAND2 aims to complete construction in 2027 and resume geoneutrino observation in 2028 !

Summary

- The KamLAND experiment has been measuring geoneutrinos from uranium and thorium.
- The reactor-off period in Japan supressed the reactor neutrino background significantly and enabled a spectropic measurement of geoneutrinos from uranium and thorium.
- Implementation of GBDT improved IBD selection efficiency from ~60% to ~70% in geoneutrino energy region (low-reactor period)
- KamLAND is now under refurbishment and aims to resume geoneutrino observation in 2028.

Backup slides

What formed our planet ?

Credit: Getty Images/iStockphoto

Traditional geoscientific approaches

Seismology

Structual modeling by earthquake analysis
"Core—mantle—crust" layers in the Earth

Geochemistry / Cosmochemistry

Compositional estimation based on rock samples and chondrite meteorites

Geothermology

Heat flux measurement at the surface etc...

Open questions

Which type of meteorites formed the Earth?
What powers the geodynamics?
How much layers the mantle have?

Geoneutrino is a key of these questions.

"Neutrino geoscience"

Structural modeling by seismology

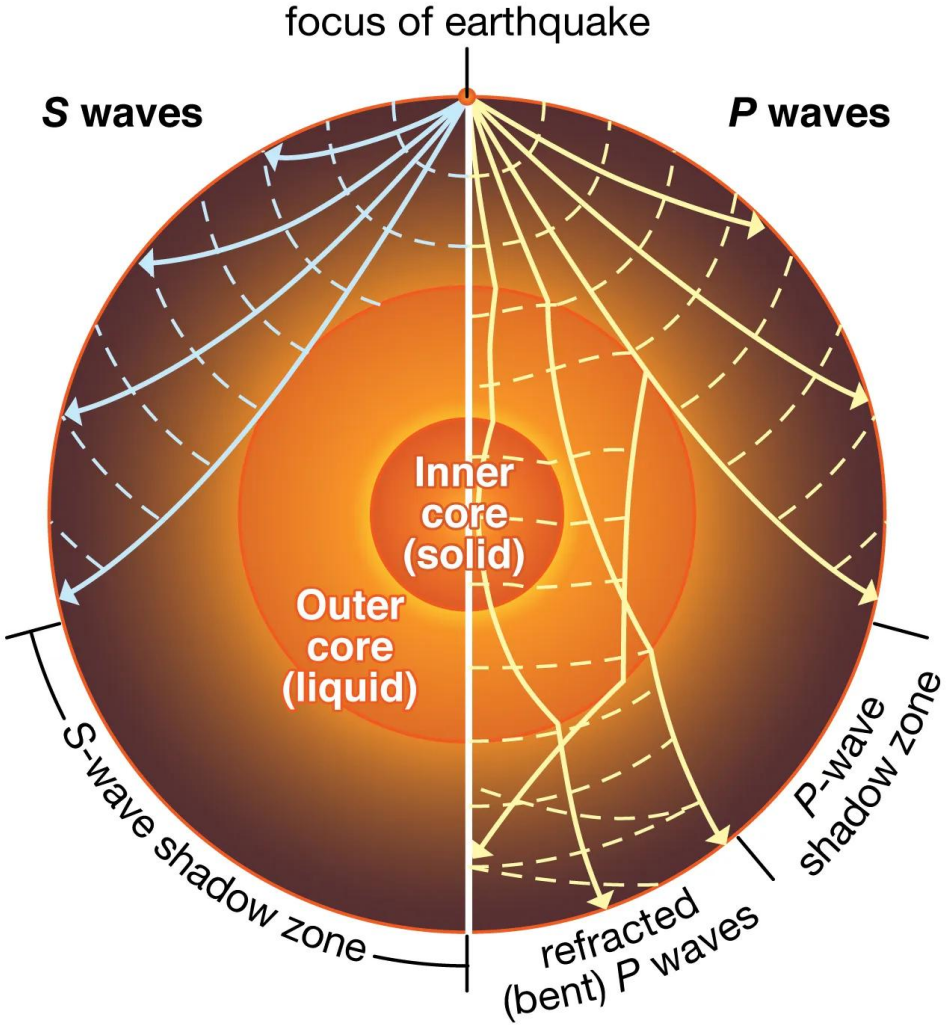

© Encyclopædia Britannica, Inc.

Multi-point observation of earthquakes propagating through the Earth

- ✓ Density and viscosity profiles of deep earth
  Multi layer of core–mantle–crust
- ? **No compositional information**

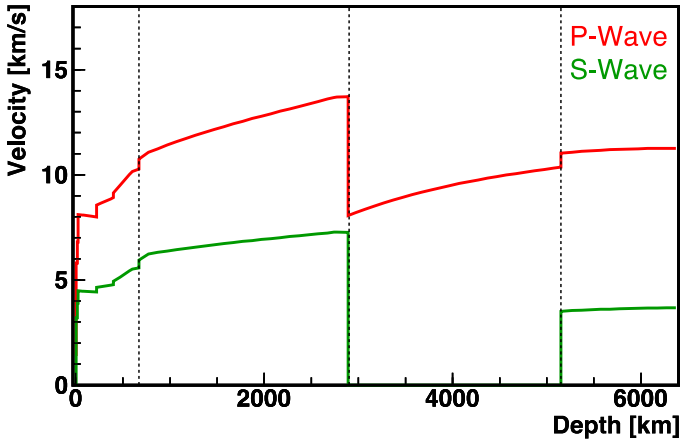

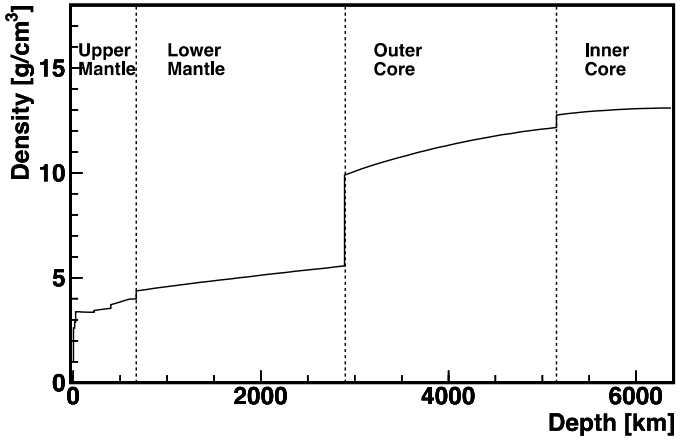

Compositional modeling by geo(cosmo)chemistry

CI carbonaceous chondrite

Enstatite chondrite

Earth's chemical composition estimate based on chondrite meteorites and earth samples

Bulk-Silicate Earth (BSE) model give average composition of mantle+crust.

Earth samples give crustal compositional estimation.

The mantle composition is estimated by subtracting crustal elements from the BSE composition.

Candidate material of the Earth : chondrites

CI carbonaceous chondrite :
- compositional similarity to solar atmosphere
- abundant volatile elements

Enstatite chondrite :
- isotopic similarity to the Earth
- abundant iron

We do never know which chondrite formed the Earth.
There be never direct sampling of deep earth.

→ Direct verification is needed.

Geothermal evolution and geodynamics

©National geographic

©全日本防災計画協会

Ref : Arevalo et al. 2009

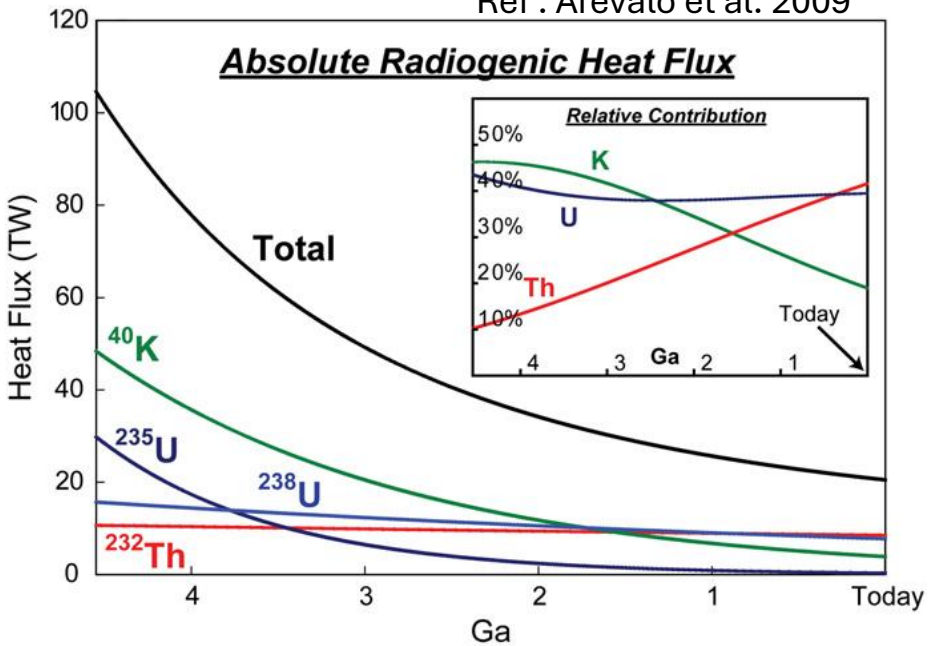

Earth heat budget

The history of the Earth is a global cooling process.
The geodynamics are powered by heat inside the Earth.

Understanding the heat amount and source inside the Earth is quit important.

Surface heat flux measurement

Bore-hole heat measurement
Total heat flux is 47±2 TW.
Source : primordial heat + radiogenic heat

? **The breakdown is unknown.**

Radiogenic heat

Heat generate by radioactive elements
Past amount is calculated from the present value.

? **Important for understanding the geothermal evolution**
Different prediction from geophysics and geochemistry

→ Direct measurement is necessary.

Motivation of geoneutrino observation

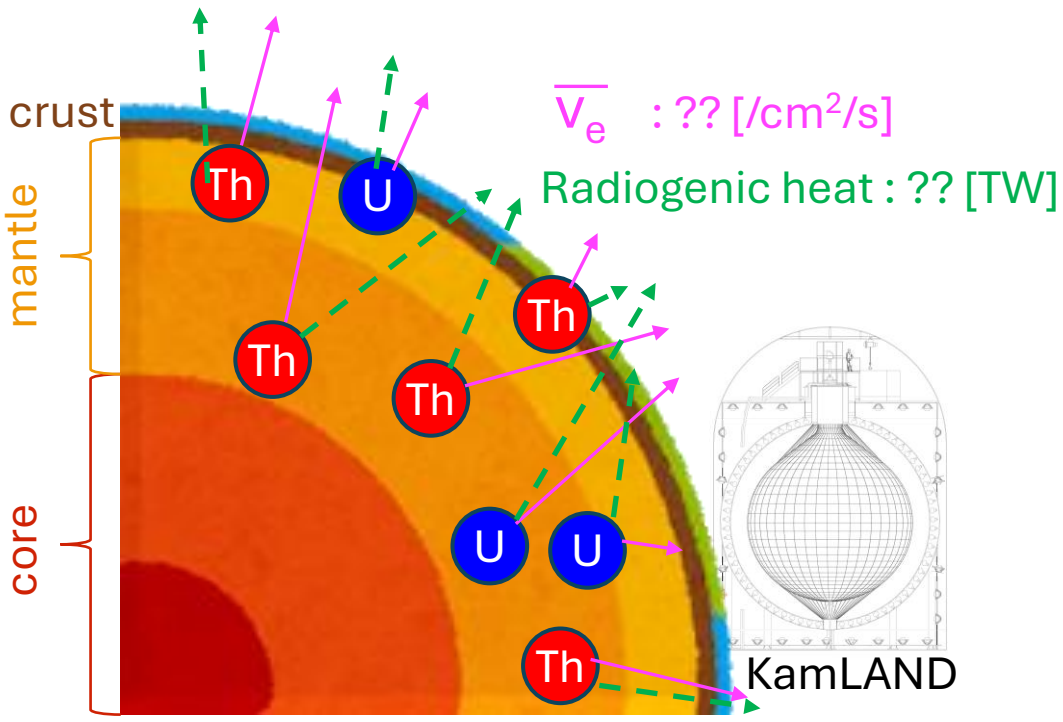

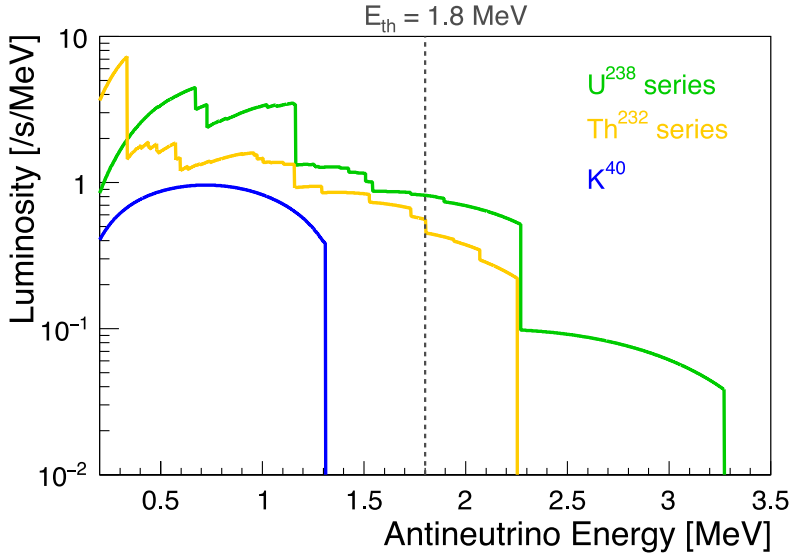

Emission of $\overline{\nu}_e$ from U, Th and K.

$$^{238}\mathrm{U} \rightarrow {}^{206}\mathrm{Pb} + 8\alpha + 6\mathrm{e}^- + 6\overline{\nu}_e + 51.7\ \mathrm{MeV}$$

$$^{232}\mathrm{Th} \rightarrow {}^{208}\mathrm{Pb} + 6\alpha + 4\mathrm{e}^- + 4\overline{\nu}_e + 42.7\ \mathrm{MeV}$$

$$^{40}\mathrm{K} \rightarrow {}^{40}\mathrm{Ca} + \mathrm{e}^- + \overline{\nu}_e + 1.311\ \mathrm{MeV}$$

Geoneutrino total flux

$\overline{\nu}_e$ flux $\propto$ U, Th $\propto$ Radiogenic heat

Test of Earth's heat budget

Geoneutrino spectrum

U and Th have different $\overline{\nu}_e$ energy.

Test of Earth's chemical composition

Broad scientific objectives of KamLAND

10^{-1} 10^{0} 10^{1} 10^{2} 10^{3} Neurino energy [MeV]

Solar neutrinos

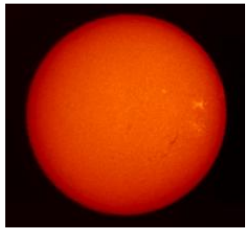

Solar mechanism
Evolusion of slars

Neutrino astronomy

Reactor neutrinos

Neutrino oscillation

Nature of neutrinos

Astrophysical burst neutrinos

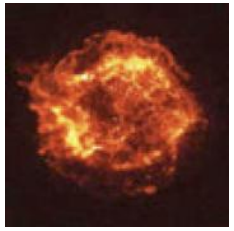

Supernova
GRB
Solar flare etc..

Neutrino astronomy

Accelerater neutrinos

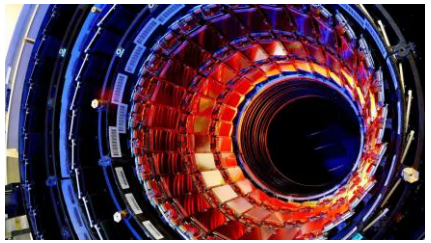

CP violation in lepton sector

Geoneutrinos

Radioactivity and heat inside the Earth

Neutrino geoscience

Neutrino provides unique probe of particle physics, astronomy and geoscience.

Geoneutrino measurement in KamLAND

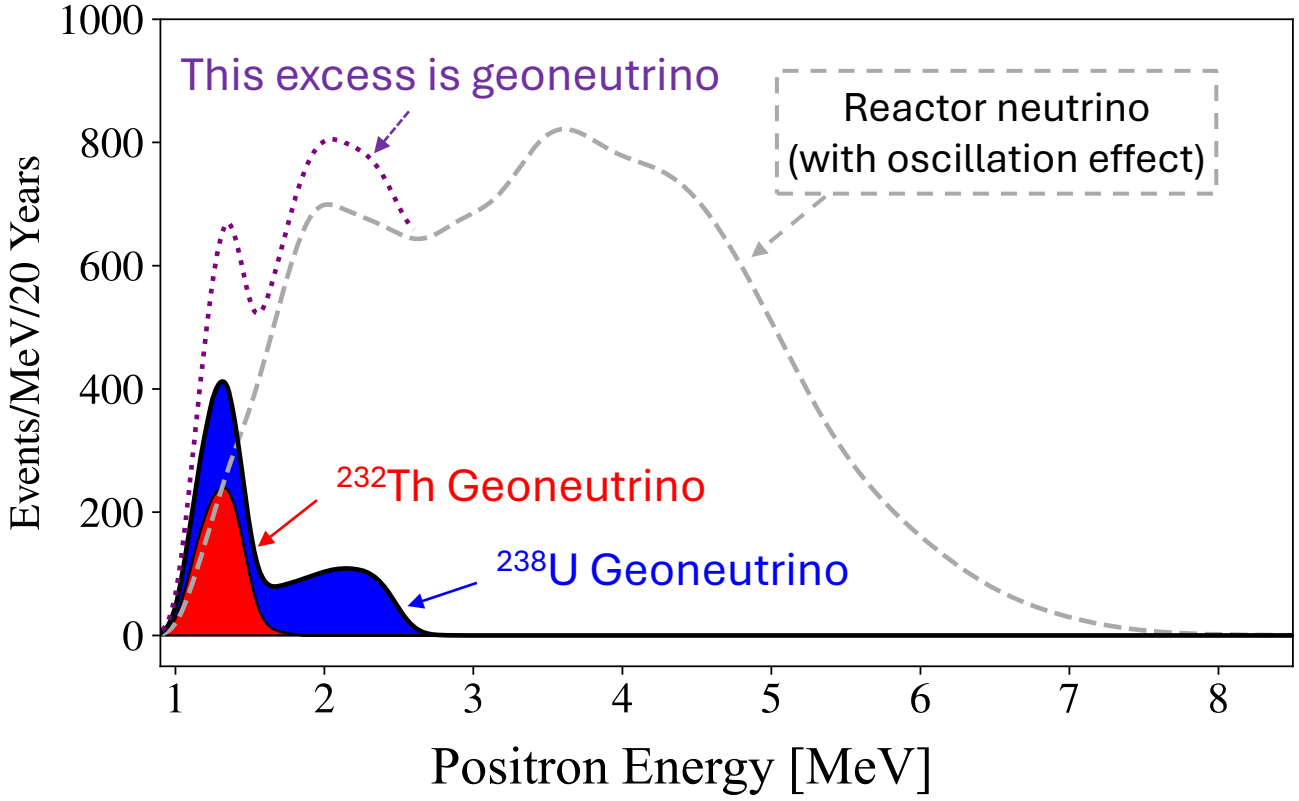

How does KamLAND measure geoneutrinos?

- KamLAND can measure rate and energy of neutrinos.
- Reactor neutrinos are the dominant background due to shared energy range.
- We can distinguish geoneutrinos from other neutrinos statistically by apllying energy (and time) spectrum fitting.

Large statistics and reduction of systematic uncertainties are very important.

It is also important to construct detector away from reactors.

Geoneutrino flux estimate

Flux estimate

The flux at the surface is calculated from knowledges of particle physics and geoscientific parameters.

Decay rate

concentration

density

$$\frac{\mathrm{d}\Phi}{\mathrm{d}R} = \sum_{i\in \mathrm{U,Th}} A_i \cdot N_i \int_{\mathrm{earth}} \mathrm{d}^3\vec{r'} \frac{a_i(\vec{r'})\rho(\vec{r'})}{4\pi|\vec{r}-\vec{r'}|^2} P(|\vec{r}-\vec{r'}|)\cdot\delta(|\vec{r}-\vec{r'}|-R)$$

Neutrino luminosity per decay

Survival probability

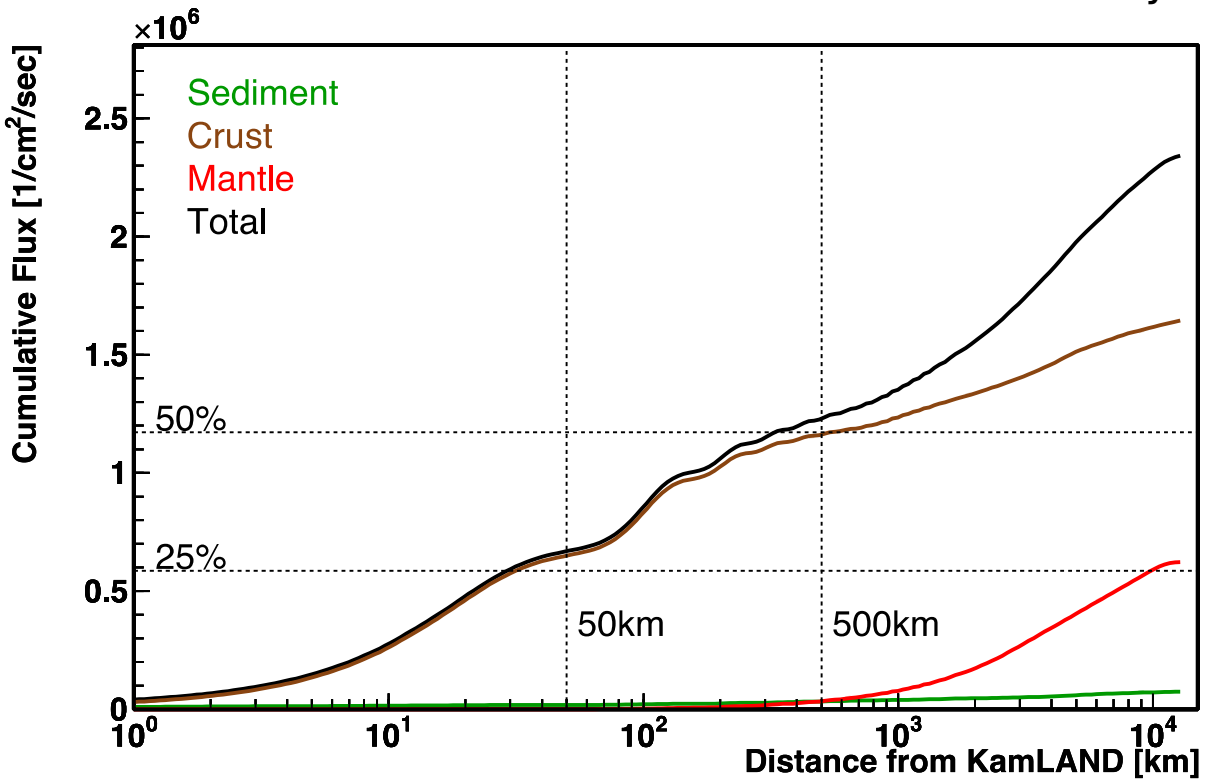

Our reference estimation (Enotomo et al 2007)

~ 70%

~27%

~ 3%

Crust / Sediment

- Based on geo(cosmo)chemical studies
- Local geological effect was averaged.
- The dominant uncertainty came from U,Th concentration measurement.

Mantle

- Subtraction of crust+sediment from BSE compositional model (M&S2003)
- We test this with geoneutrino

Neutrino oscillation measurement

KamLAND can detect neutrinos from reactors with average distance of 180 km.

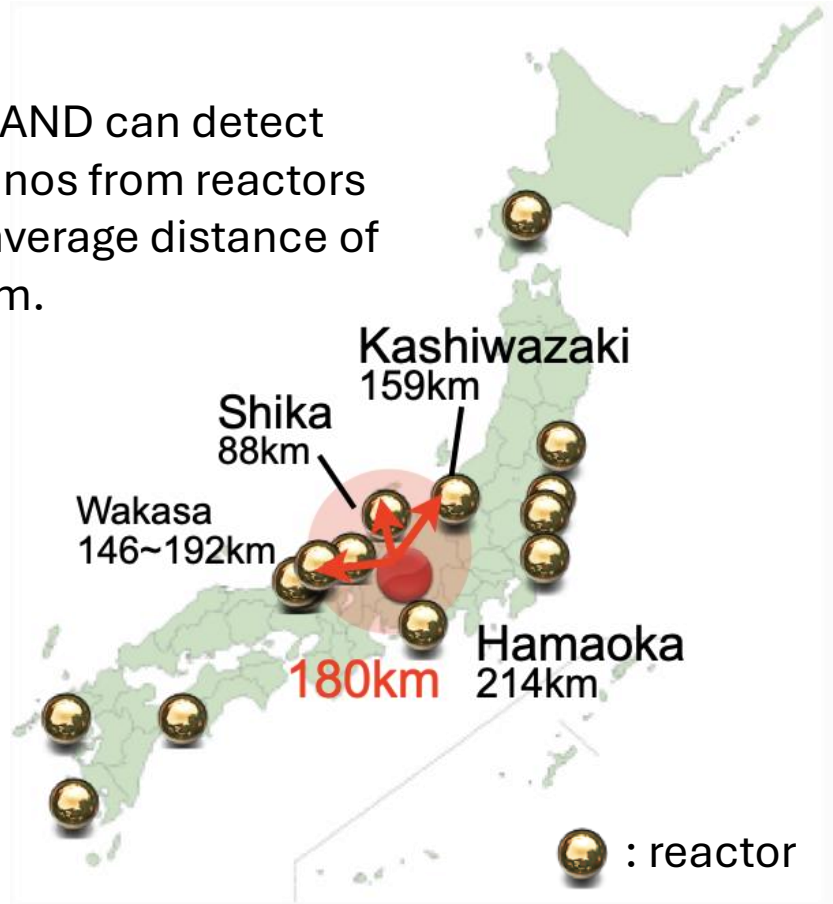

Two-flavor survival probability is appximated as

$$\widetilde{P}_{ee}^{2\nu} = 1 - \sin^2\left(2\widetilde{\theta}_{12}\right)\sin^2\left(\frac{\Delta\widetilde{m}_{21}^2 L}{E_\nu}\right)$$

$\widetilde{\theta}_{12}, \widetilde{m}_{21}$: ν_1-ν_2 oscillation parameters in earth

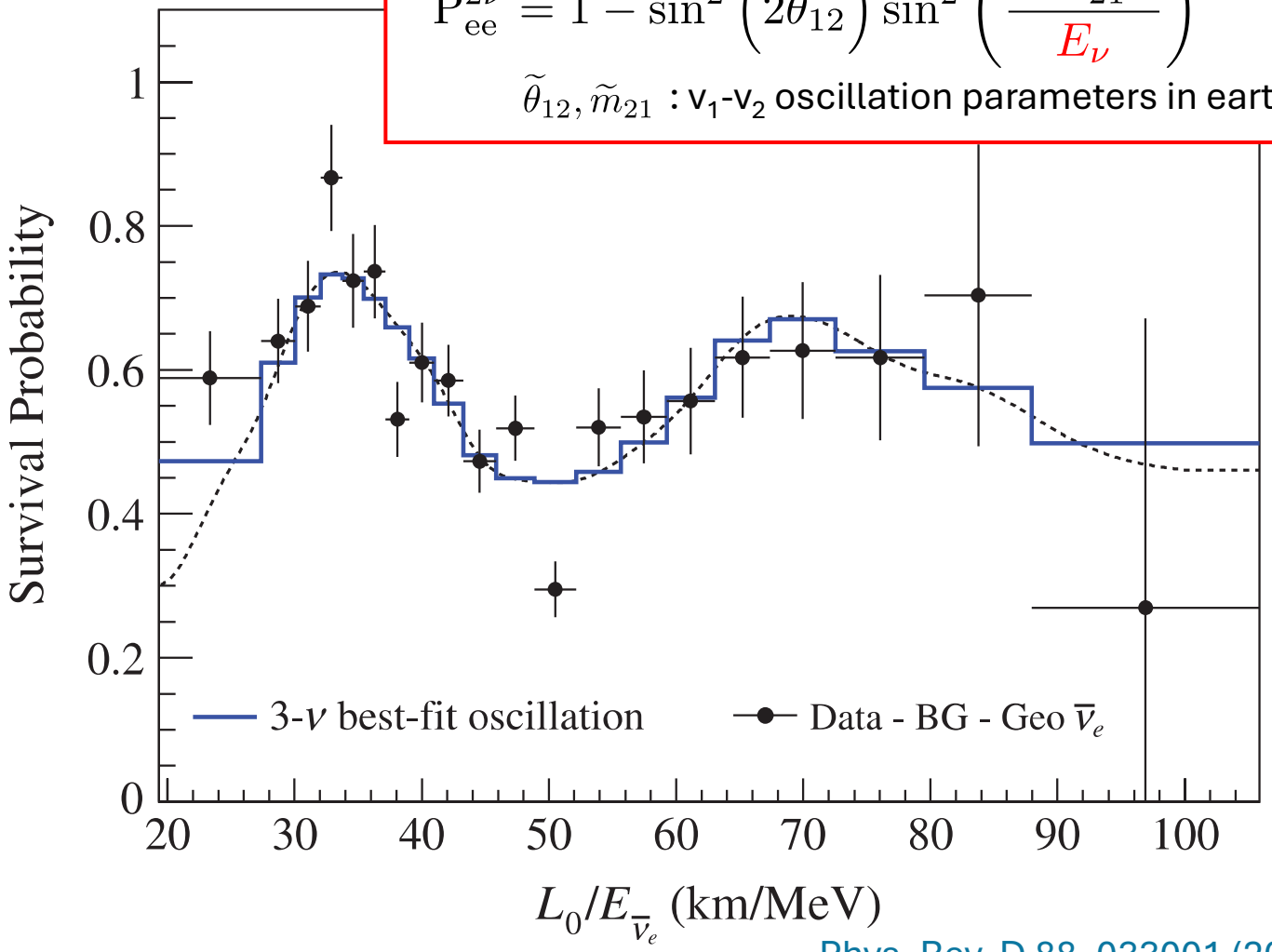

Phys. Rev. D 88, 033001 (2013)

KamLAND measured 2 cycles of neutrino oscillation precisely for the first time in the world.

Liquid scintillator purification with distillation

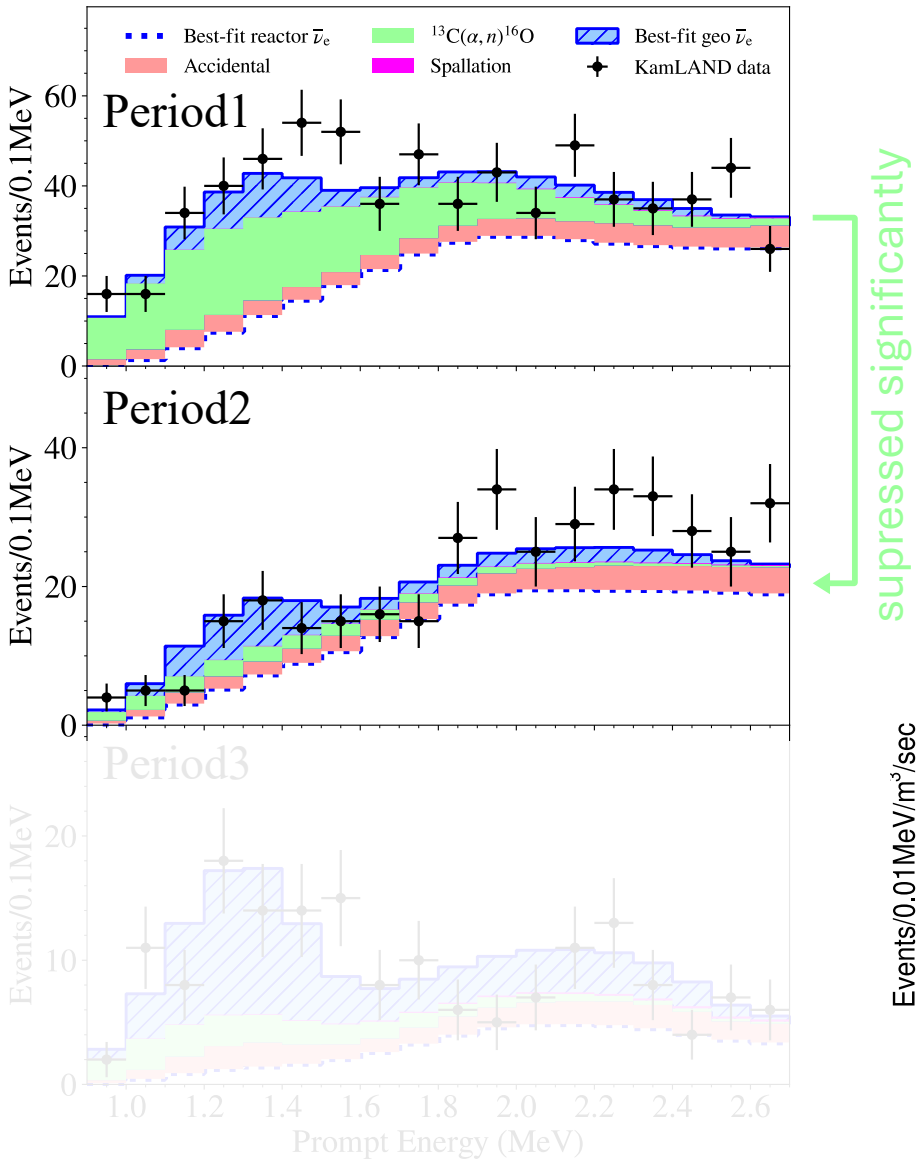

$^{13}C(\alpha,n)^{16*}O$ background

- Mimic neutrino signal
- Triggered by α particle
- Main α source : ^{210}Po
- Main ^{210}Po source : ^{210}Pb

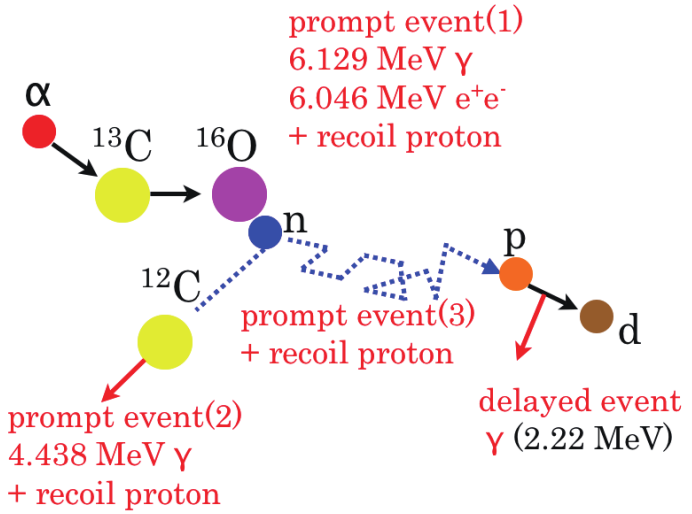

Reduction of ^{210}Pb by distillation campaigns in 2007 and 2008

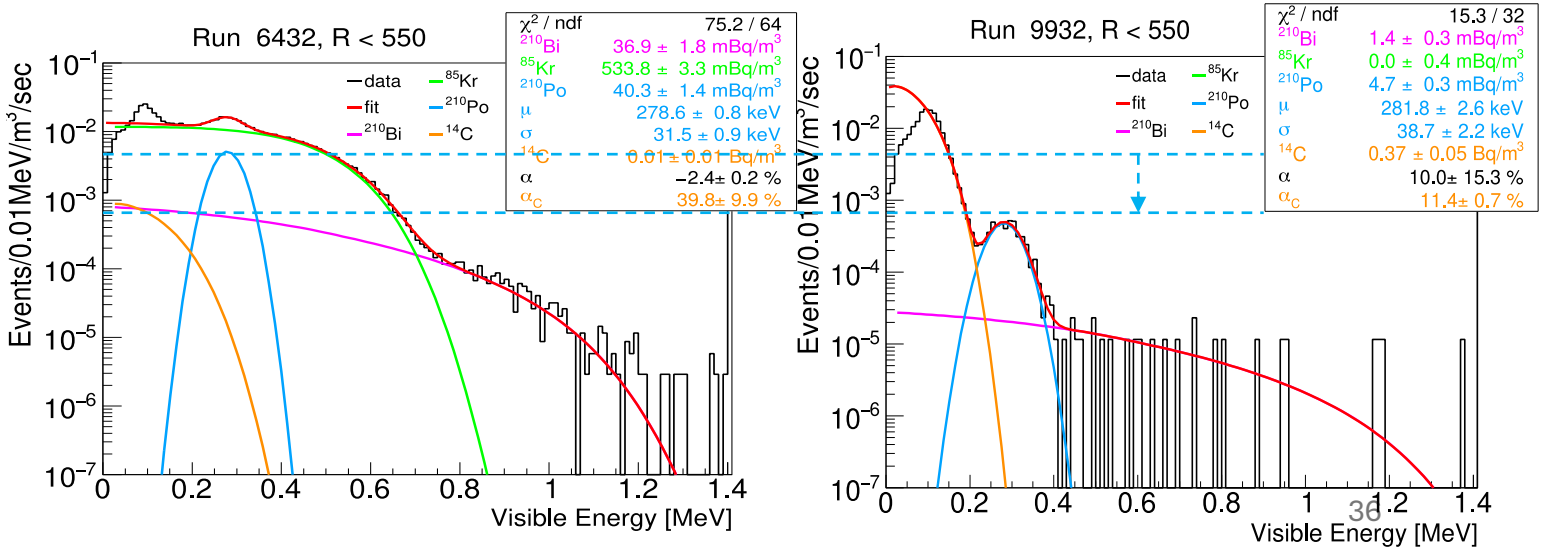

Impact of reactor-off period

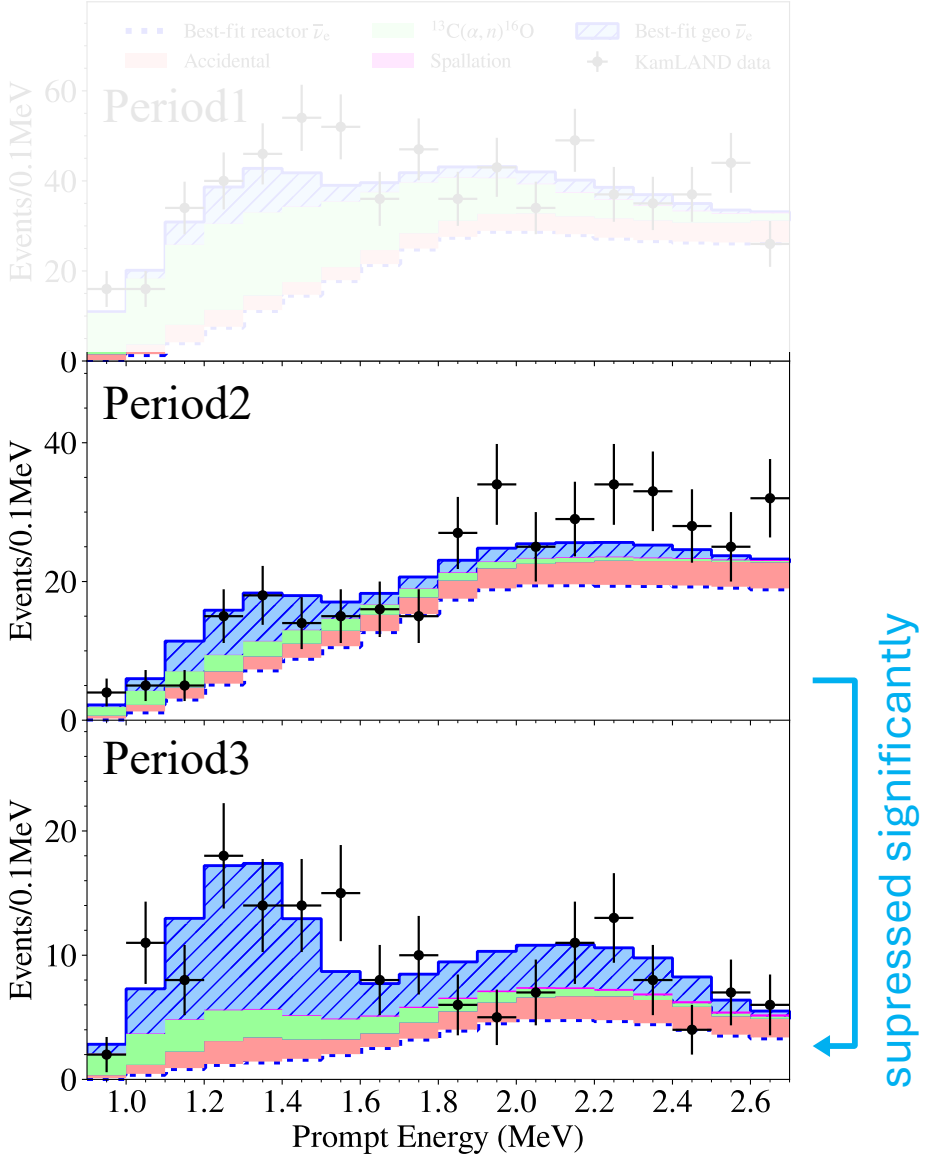

Reactor neutrino background

- Significantly decreased due to the reactor-off environment

Accidental-coincidence background

- Suppressed by optimization of likelihood-based anti-neutrino event selection in reactor-off period.

Geoneutrino signal

- In the reactor-off period, the spectrum shape can be seen clearly.

Statistical power of reactor-off period

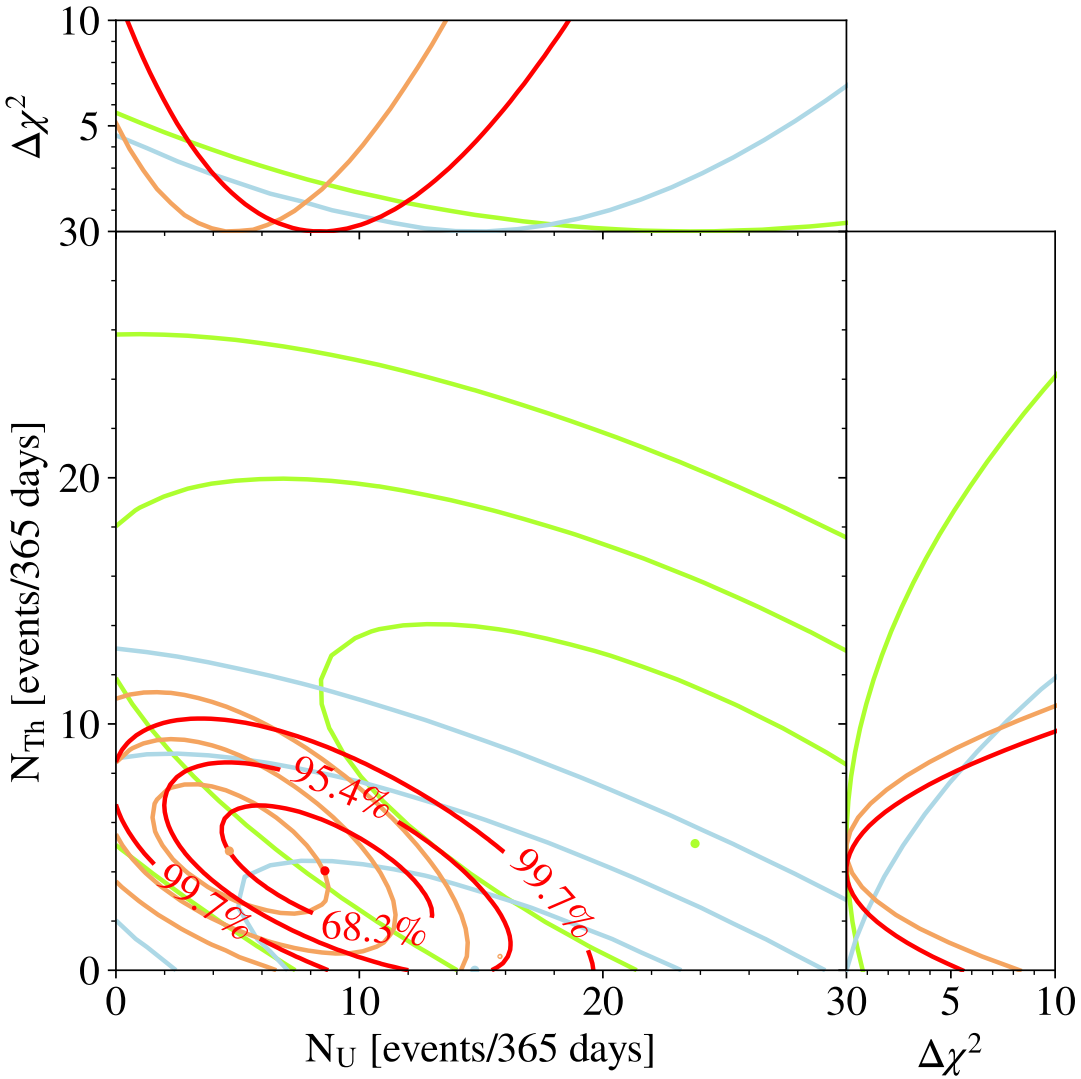

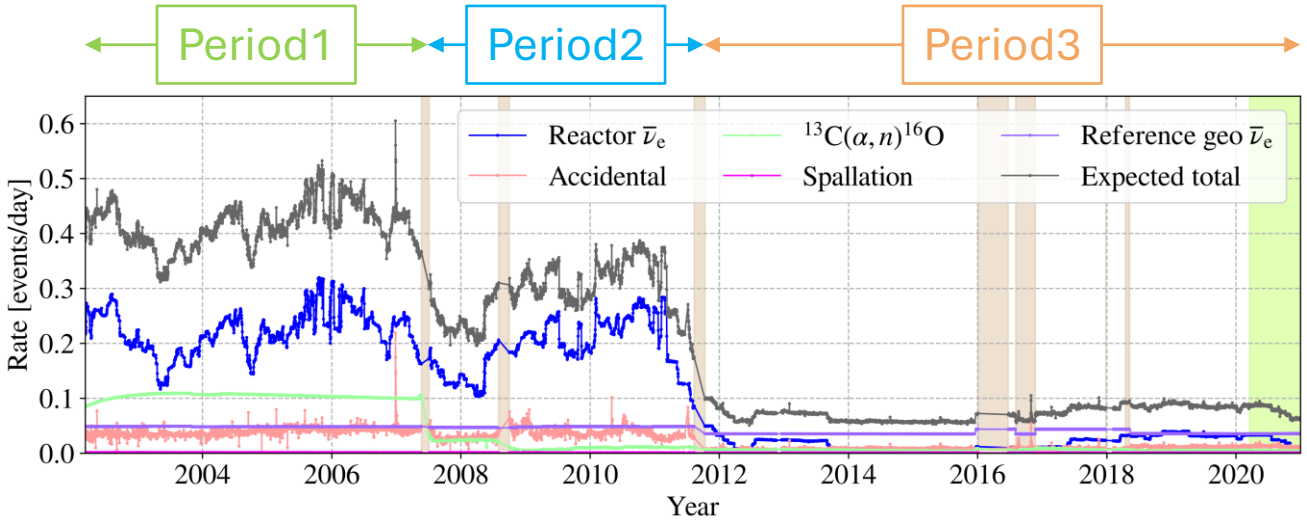

Period3 (reactor-off period) contributes to the determination of geoneutrino flux from Uranium and Thorium.

Conventional IBD selection

Likelihood selection threshold

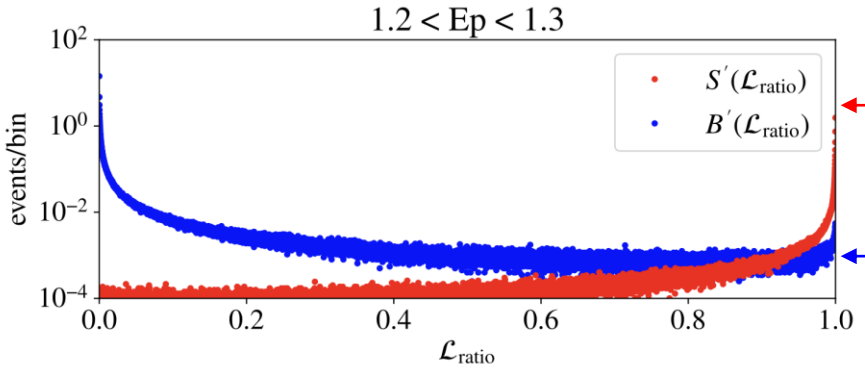

Geant4-simulate $\mathcal{L}_{\rm ratio}$ distribution in IBD

Data-driven $\mathcal{L}_{\rm ratio}$ distribution in accidental-coincidence

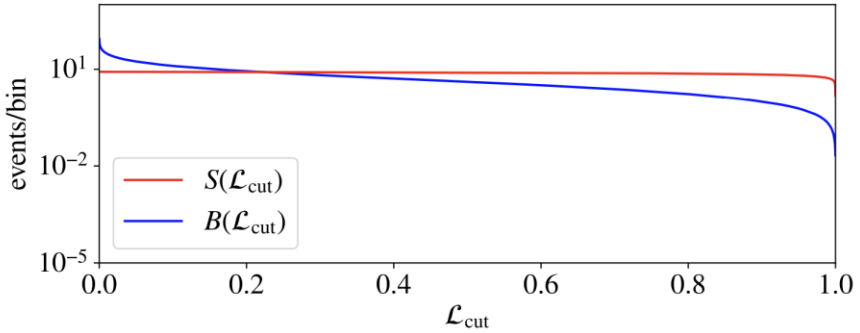

Right-side integral of $\mathcal{L}_{\rm ratio}$ = Remaining events if we apply a cut $\mathcal{L}_{\rm ratio} > \mathcal{L}_{\rm cut}$

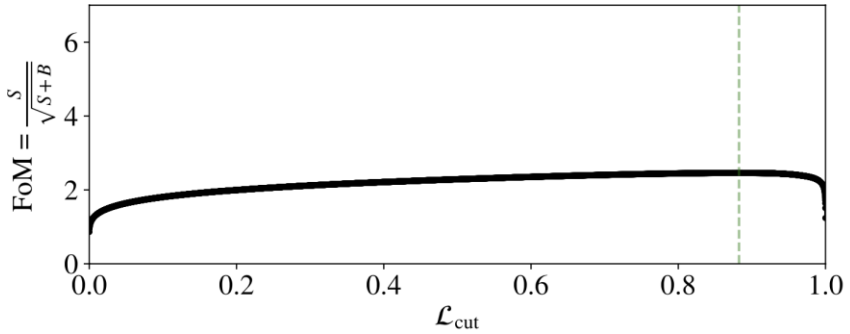

$$\mathrm{FoM}(\mathcal{L}_{\rm cut}) = \frac{S(\mathcal{L}_{\rm cut})}{S(\mathcal{L}_{\rm cut}) + B(\mathcal{L}_{\rm cut})}$$

The best $\mathcal{L}_{\rm cut}$ maximize this FoM.

Conventional IBD selection

N-1 plot

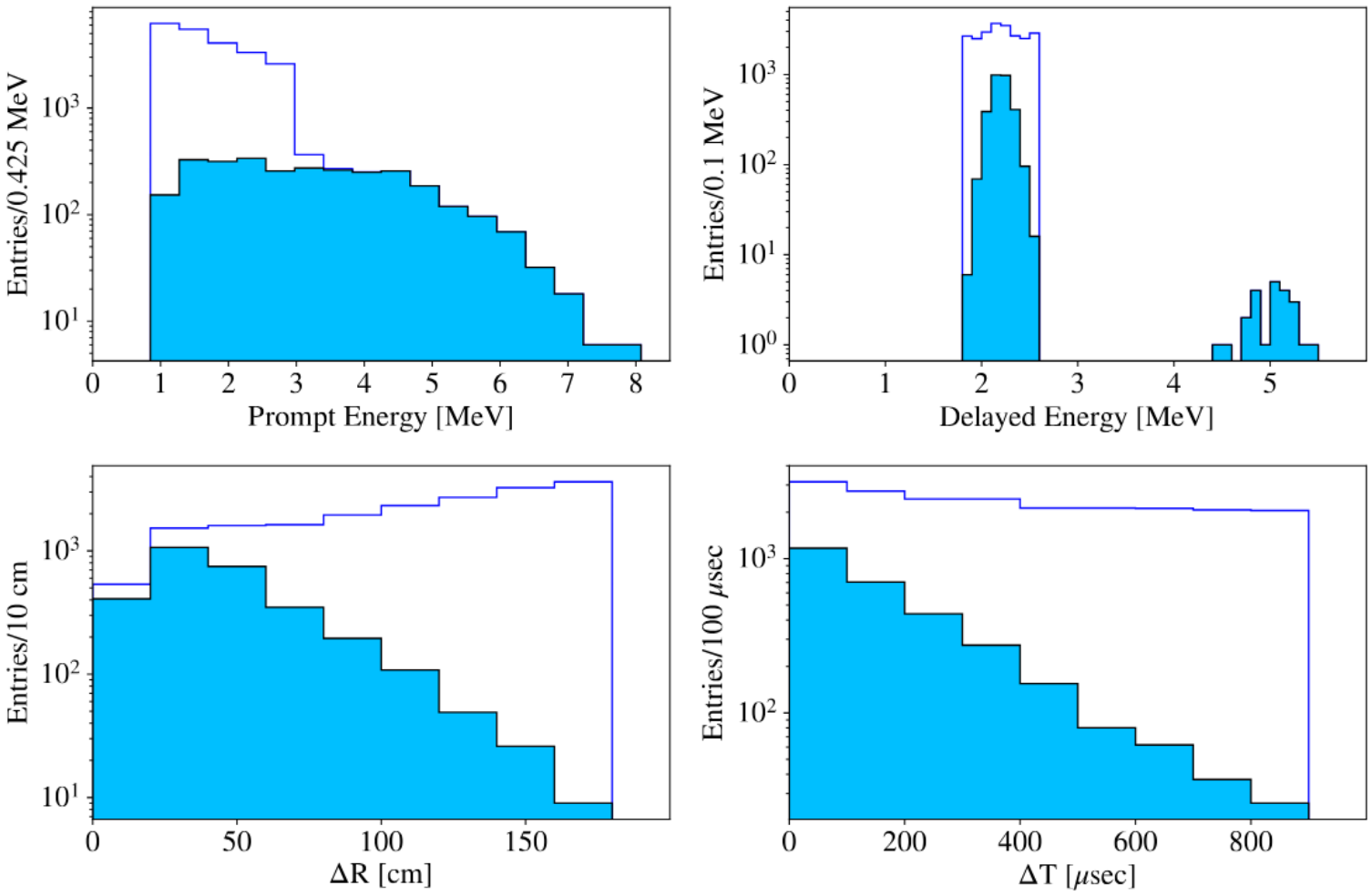

Accidental-coincidence background

Only delayed-coincidence

parameter	criteria
prompt energy [MeV]	$0.9 \leq E_p < 8.5$
delayed energy [MeV]	$1.8 \leq E_d < 2.6$ $4.4 \leq E_d < 5.6$
space correlation [m]	$\Delta R < 2.0$
time correlation [μs]	~~$0.5 \leq \Delta T < 1000$~~
fiducial volume [m]	$R_p < 6$ & $R_d < 6$

0.2–1.2 [sec]

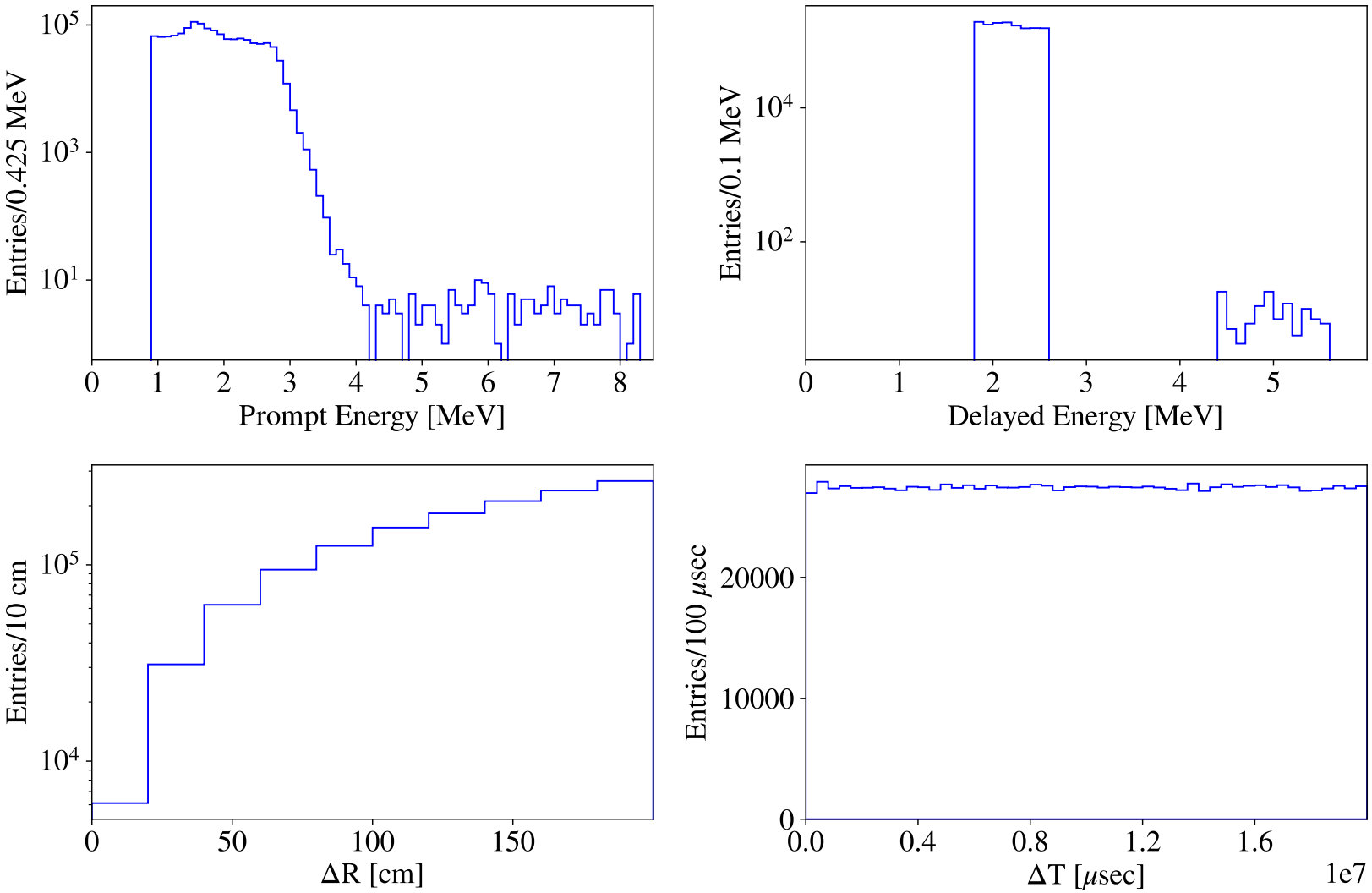

Accidental-coincidence background

Delayed-coincidence only

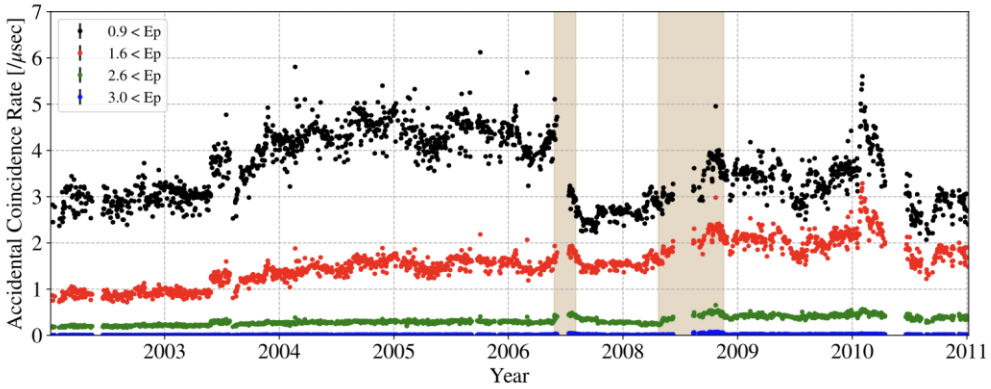

Figure 5.16: Time variation of the accidental coincidence rate in Period1 and Period2. The accidental coincidence events are selected by the delayed-coincidence method and the likelihood selection has not been applied.

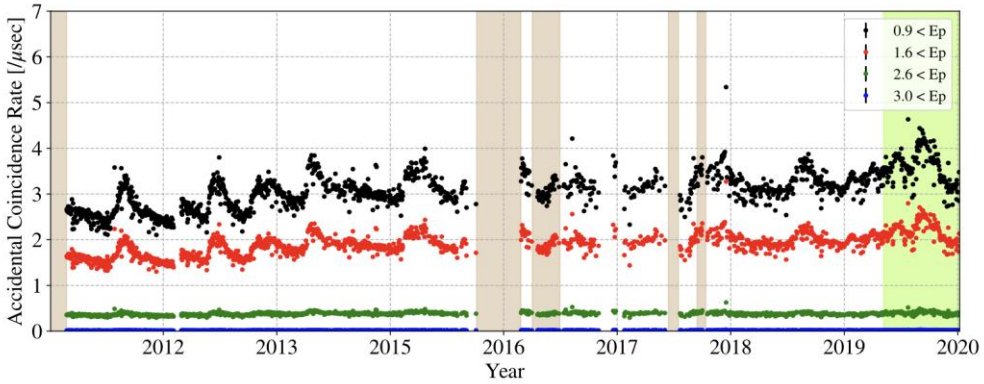

Figure 5.17: Time variation of the accidental coincidence rate in Period3. The accidental coincidence events are selected by the delayed-coincidence method and the likelihood selection has not been applied.

Likelihood selection applied

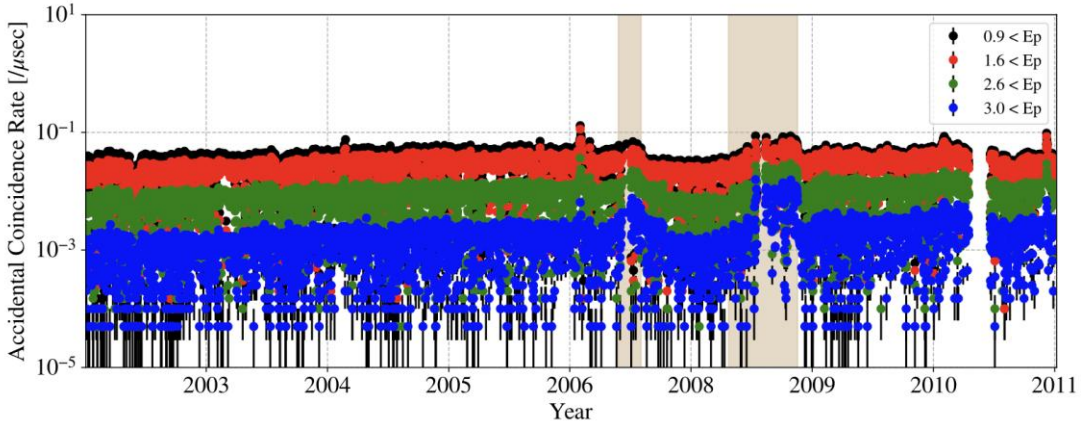

Figure 6.43: Time variation of the accidental coincidence background rate after Likelihood cut in Period1 and Period2.

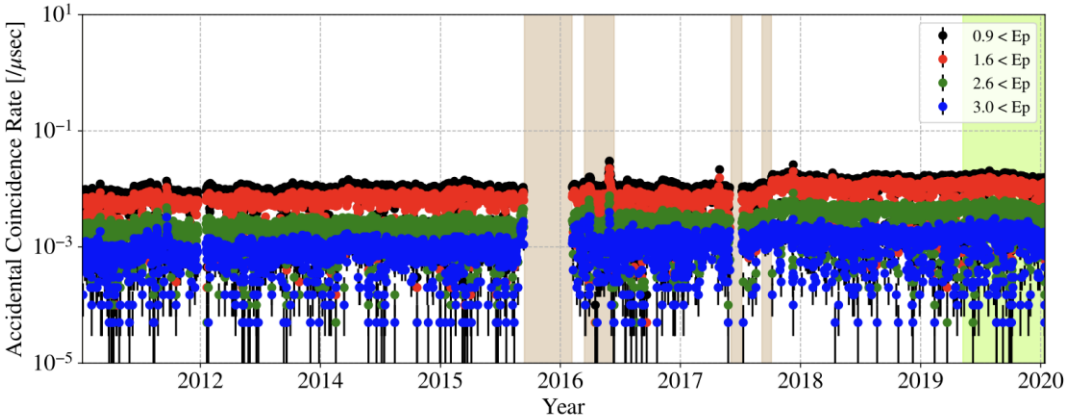

Figure 6.44: Time variation of the accidental coincidence background rate after Likelihood cut in Period3

Why acci. BG was suppressed in period3 ?

‘02/Mar./9–’03/Oct./31 (period1)

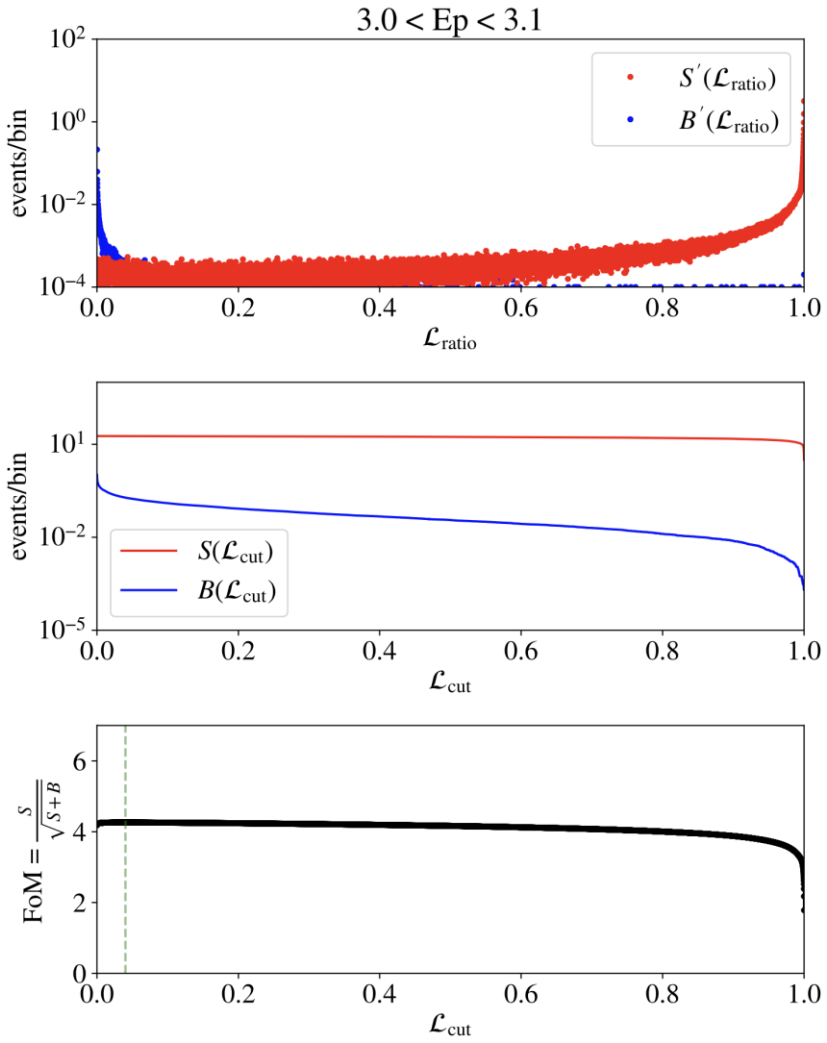

Figure 5.20: Likelihood selection procedure for $3.0 < E_{\rm p} < 3.5$ in LH-0

Fewer IBD expectation in reactor-off period

Accidental coincidence rate does not change in reactor-off period

The optimized threshold shifted to right.

Higher threshold suppressed more accidental background.

‘18/May/19—’20/Dec./31 (Period3)

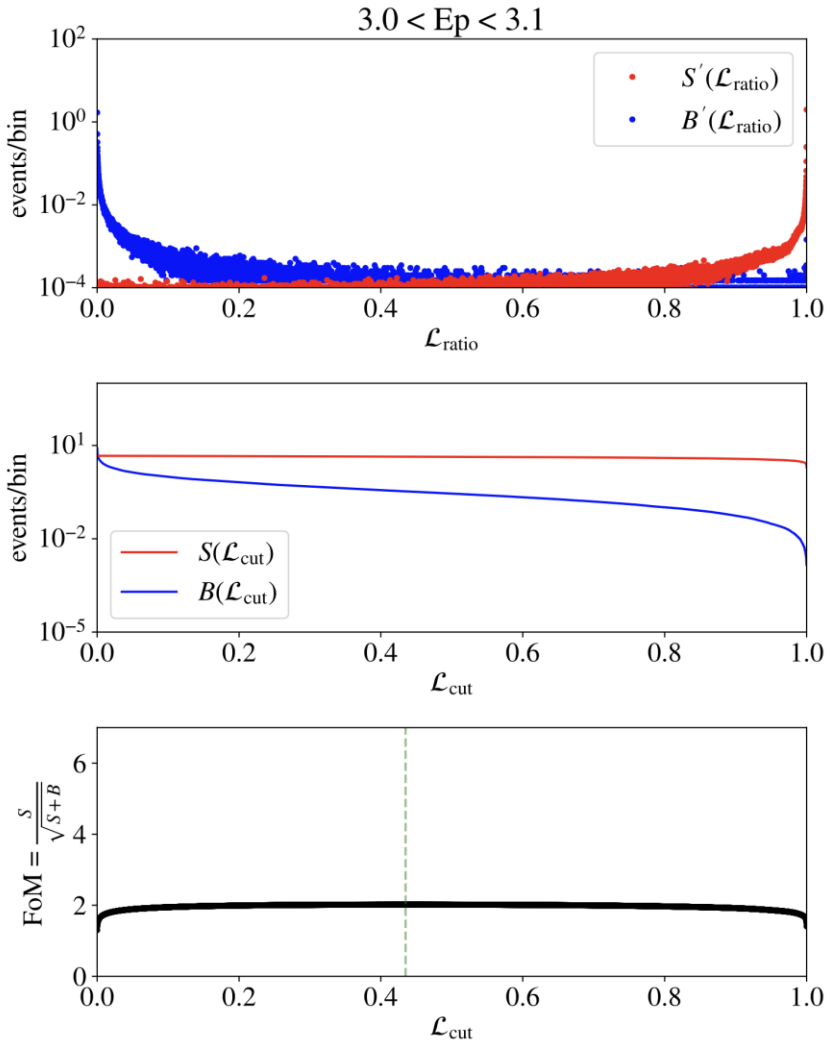

Figure 5.23: Likelihood selection procedure for $3.0 < E_{\rm p} < 3.5$ in LH-7

Comparison to Earth models

Tension between KamLAND data and models

$$\chi^2_{\rm min} = \min_{(\alpha^{\rm U}_{\rm crust},\alpha^{\rm Th}_{\rm crust},\alpha_{\rm BSE})} \left\{\chi^2_{\rm KL}(\Phi^{\rm U}_{\rm crust} + \Phi^{\rm Th}_{\rm crust} + \Phi_{\rm mantle}) + \chi^2_{\rm penalty}\right\}$$

$$\Phi_{\rm mantle} = \left(Q_{\rm BSE} - Q^{\rm U}_{\rm crust} - Q^{\rm Th}_{\rm crust}\right) \frac{{\rm d}\Phi^{\rm U,Th}_{\rm mantle}}{{\rm d}Q^{\rm U,Th}_{\rm mantle}}$$

$$\chi^2_{\rm penalty} = (\alpha^{\rm U}_{\rm crust})^2 + (\alpha^{\rm Th}_{\rm crust})^2 + (\alpha^{\rm Th/U}_{\rm crust})^2 + (\alpha_{\rm BSE})^2$$

Constraints from crust and BSE models

$$\alpha^{\rm U}_{\rm crust} = \frac{Q^{\rm U}_{\rm crust} - Q^{\rm U,Model}_{\rm crust}}{Q^{\rm U,Model}_{\rm crust} \times (24\%)} = \frac{\Phi^{\rm U}_{\rm crust} - \Phi^{\rm U,Model}_{\rm crust}}{\Phi^{\rm U,Model}_{\rm crust} \times (24\%)}$$

$$\alpha^{\rm Th}_{\rm crust} = \frac{Q^{\rm Th}_{\rm crust} - Q^{\rm Th,Model}_{\rm crust}}{Q^{\rm Th,Model}_{\rm crust} \times (11\%)} = \frac{\Phi^{\rm Th}_{\rm crust} - \Phi^{\rm Th,Model}_{\rm crust}}{\Phi^{\rm Th,Model}_{\rm crust} \times (11\%)}$$

$$\alpha^{\rm Th/U}_{\rm crust} = \frac{\alpha^{\rm Th}_{\rm crust} - \alpha^{\rm U}_{\rm crust}}{\alpha^{\rm U}_{\rm crust} \times \binom{4.8\%}{3.5\%}} \qquad (\because \text{Th/U mass ratio} = 3.95^{+0.19}_{-0.13})$$

$$\alpha_{\rm BSE} = \frac{Q_{\rm BSE} - Q^{\rm Model}_{\rm BSE}}{Q^{\rm Model}_{\rm BSE} \times (10\%)} \qquad Q^{\rm Model}_{\rm BSE} = 28.2\,{\rm TW} \qquad \text{(High-Q model)}$$

	$Q^{\rm Model}_{\rm crust}$ [TW]	$\Phi^{\rm Model}_{\rm crust}$ [10^5 cm^{-2}s^{-1}]	$\frac{{\rm d}Q_{\rm mantle}}{{\rm d}\Phi_{\rm mantle}}$ [10^{-5} TW/cm^{-2}s^{-1}]
^{238}U	3.35	17.19	7.28
^{232}Th	3.61	14.51	9.32

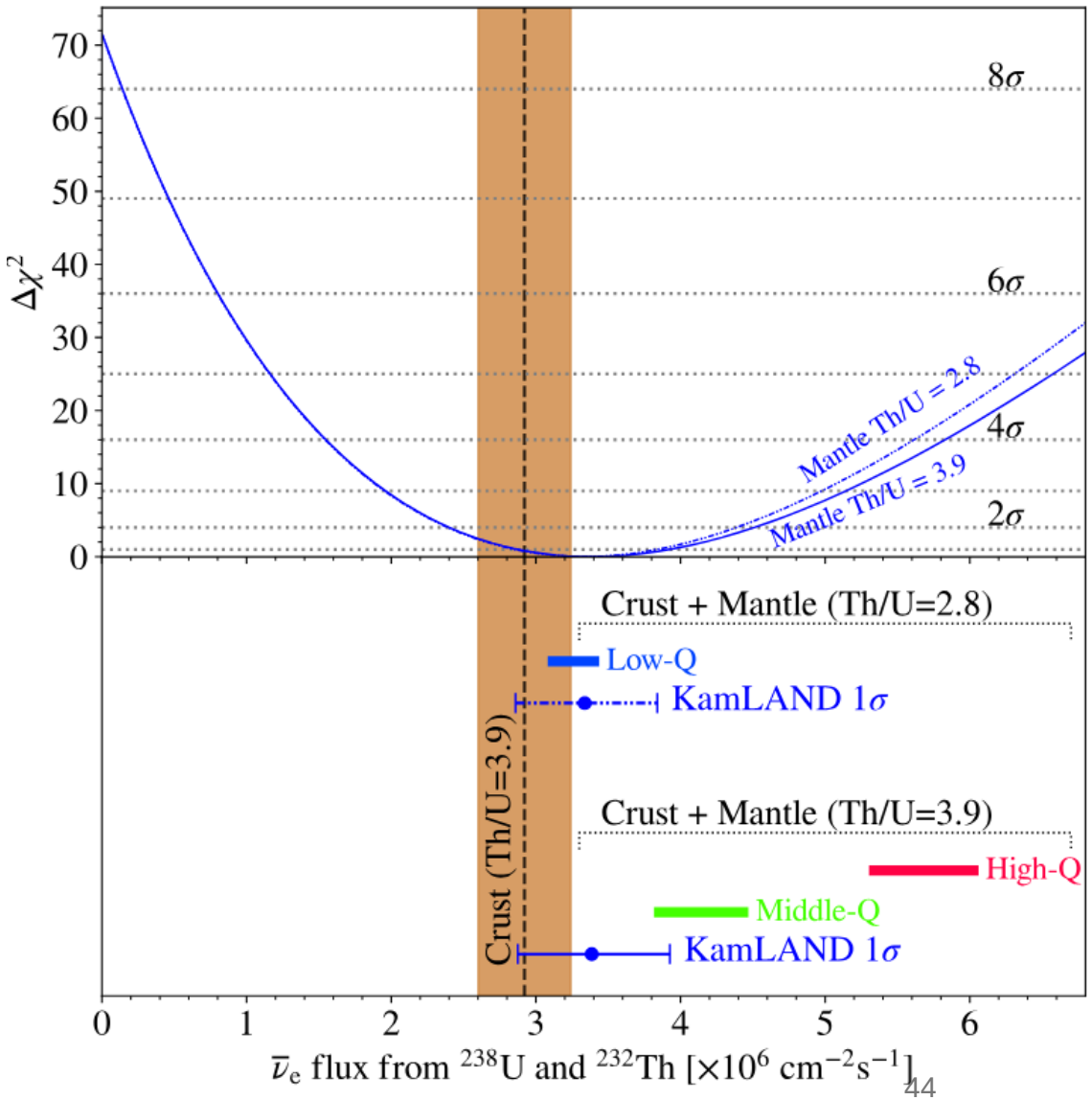

Comparison to Earth models

Assuming homogeneous mantle composition,

High-Q model is disfavored at 99.76%.

Assuming U and Th concentration at the mantle-core boundary,

High-Q model is disfavored at 97.9%.

High-Q model rationale

Seismology data → density/viscosity profile → 1-layer mantle convection
Radiogenic heat : ~25 TW

High-Q model rejection indicates the need to modify the mantle density/viscosity profile or geodynamical modeling of mantle convection.

The KamLAND data favor Low-Q, Middle-Q model.

This result suggests mantle multi-layer convection.

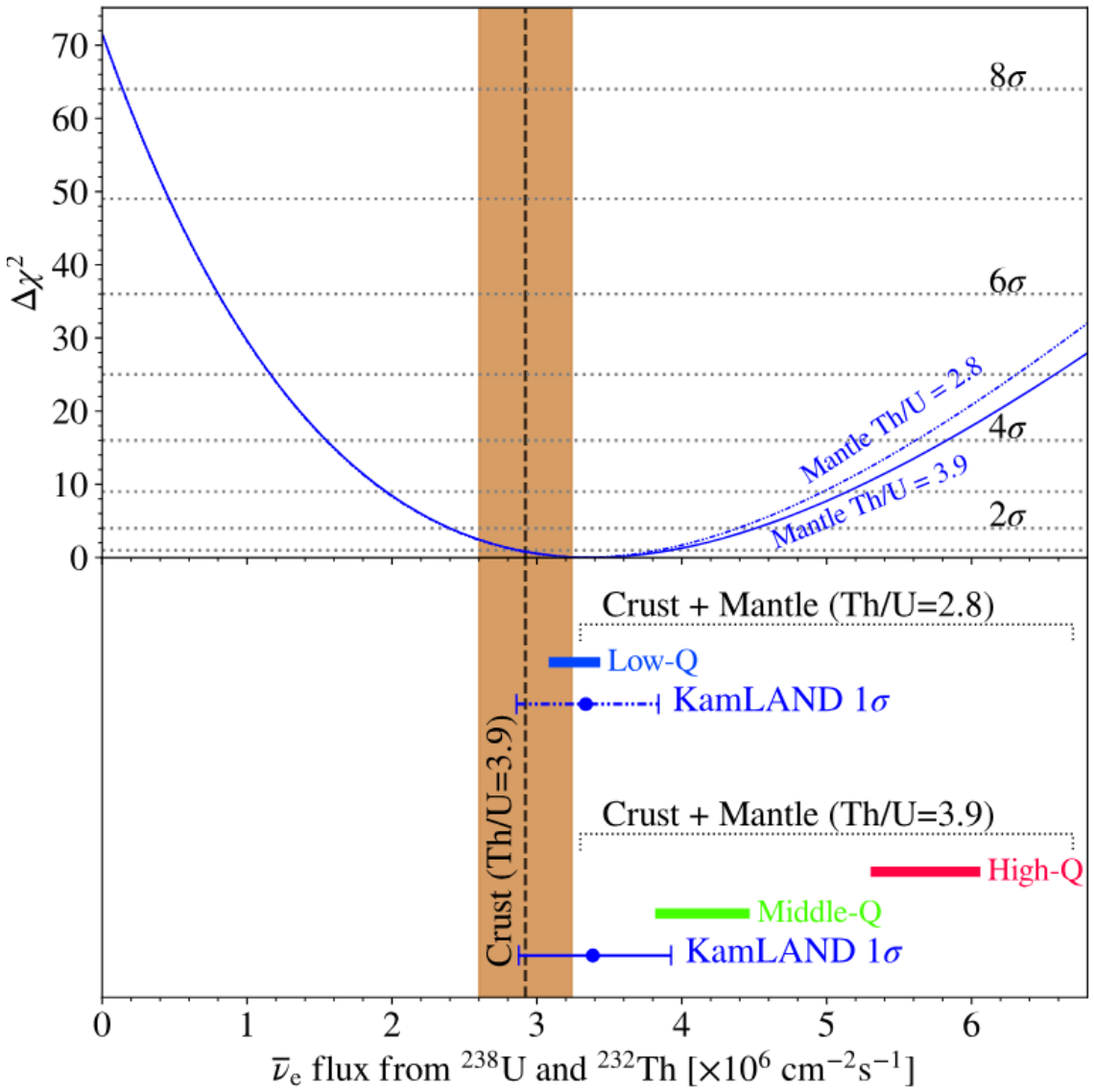

Summary

- The KamLAND experiment has been measuring geoneutrinos from uranium and thorium.

- The reactor-off period in Japan supressed the reactor neutrino background significantly and enabled a spectropic measurement of geoneutrinos from uranium and thorium.

Flux

	$N_{\mathrm{U/Th}}$ [event]	flux [$\times 10^5$ cm^{-2}s^{-1}]	flux [TNU]	0-signal rejection
U	$116.6^{+41.0}_{-38.5}$	$14.7^{+5.2}_{-4.8}$	$19.1^{+6.7}_{-6.3}$	3.343σ
Th	$57.5^{+24.5}_{-24.1}$	$23.9^{+10.2}_{-10.0}$	$9.7^{+4.1}_{-4.1}$	2.386σ
U + Th	$173.7^{+29.2}_{-27.7}$	$32.1^{+5.8}_{-5.3}$	$28.6^{+5.1}_{-4.8}$	8.3σ

Radiogenic heat

$$Q^{\mathrm{U}} = 3.3^{+3.2}_{-0.8}\ \mathrm{TW}$$
$$Q^{\mathrm{Th}} = 12.1^{+8.3}_{-8.6}\ \mathrm{TW}$$
$$Q^{\mathrm{U}} + Q^{\mathrm{Th}} = 15.4^{+8.3}_{-7.9}\ \mathrm{TW}$$

Convective Uray ratio = $0.13^{+0.15}_{-0.06}$

- The KamLAND data is consistent with Low-Q and Middle-Q model based on chondrites compositional analysis, whereas the High-Q model is disfavored at 99.76% confidence level with assuming the homogeneous mantle composition, implying multi-layer mantle convection.

Reactor neutrino spectrum

Neutrino spectrum from a reactor

IBD cross section

$$S(E_\nu) = S_{DB}(E_\nu) + \sum_{x \in \text{isotope}} (f_i^x - f_{DB}^x) S_{HM}^x(E_\nu) \sigma_{IBD}(E_\nu)$$

Differences in fission fraction of major isotopes

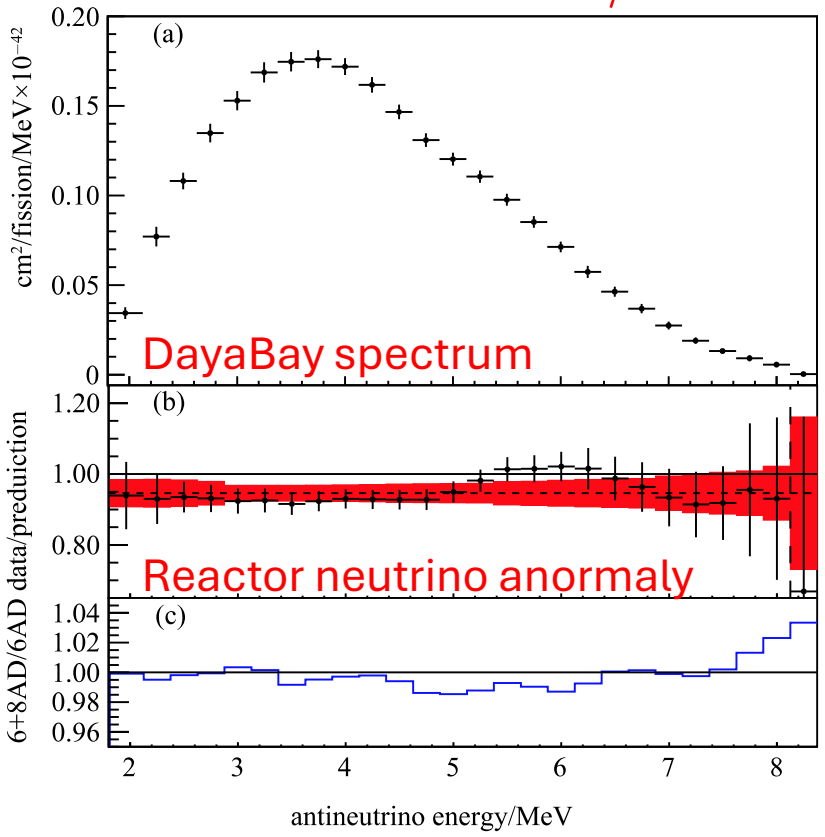

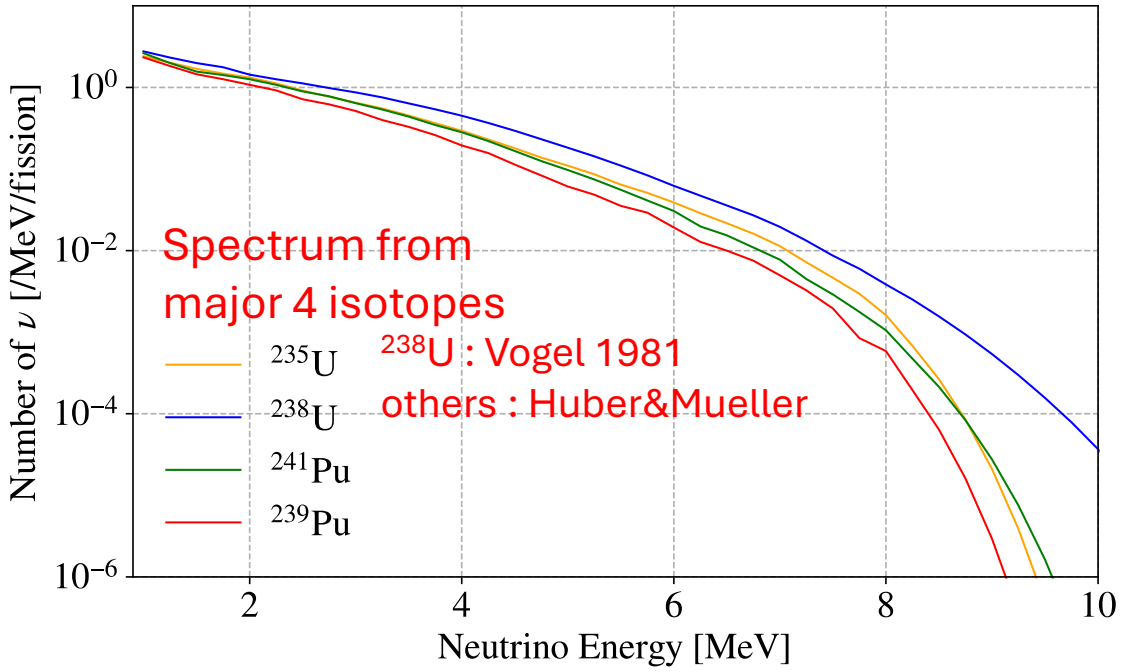

Improvement in IBD selection efficiency

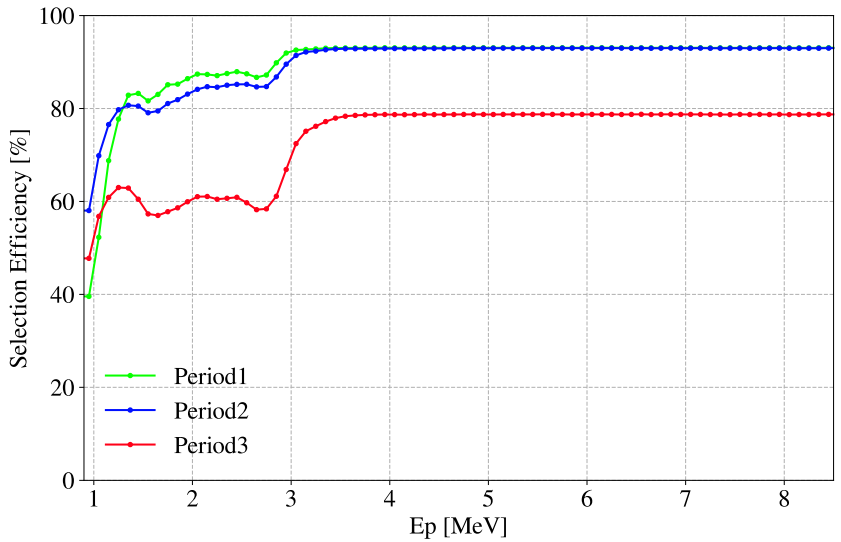

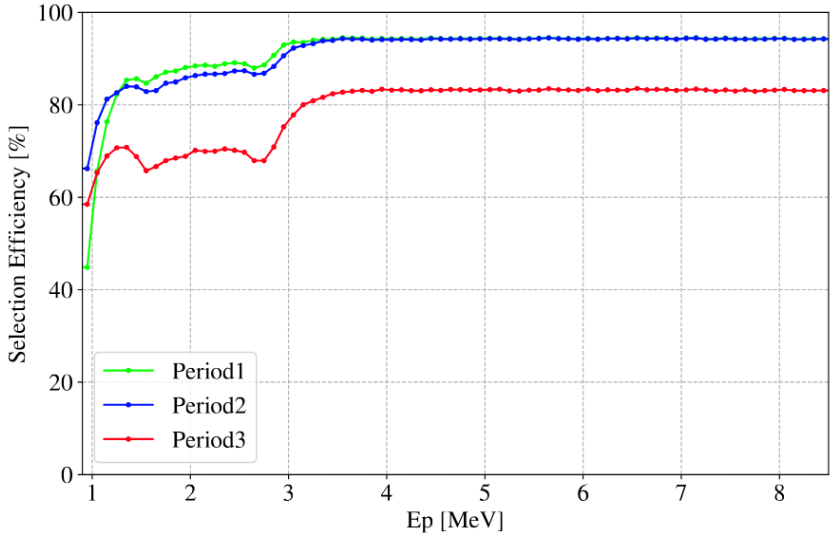

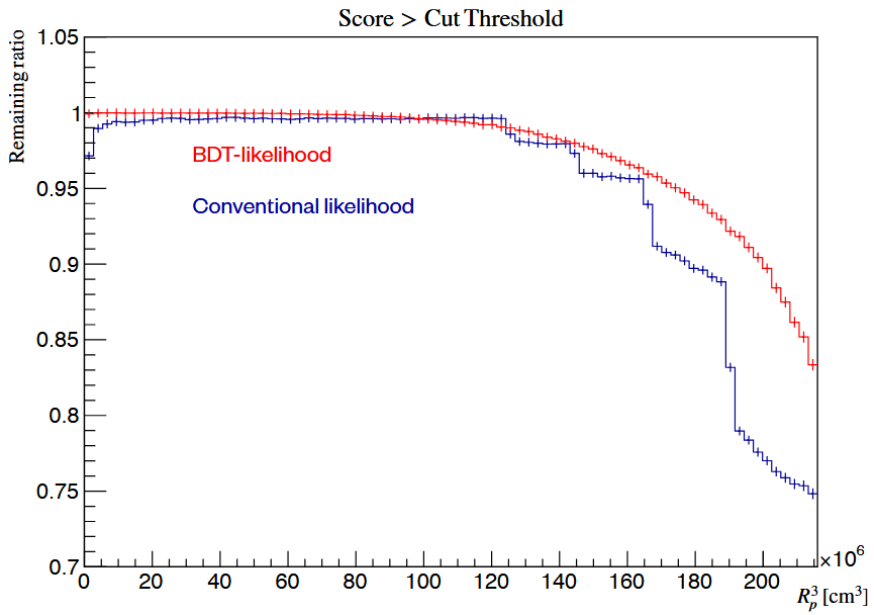

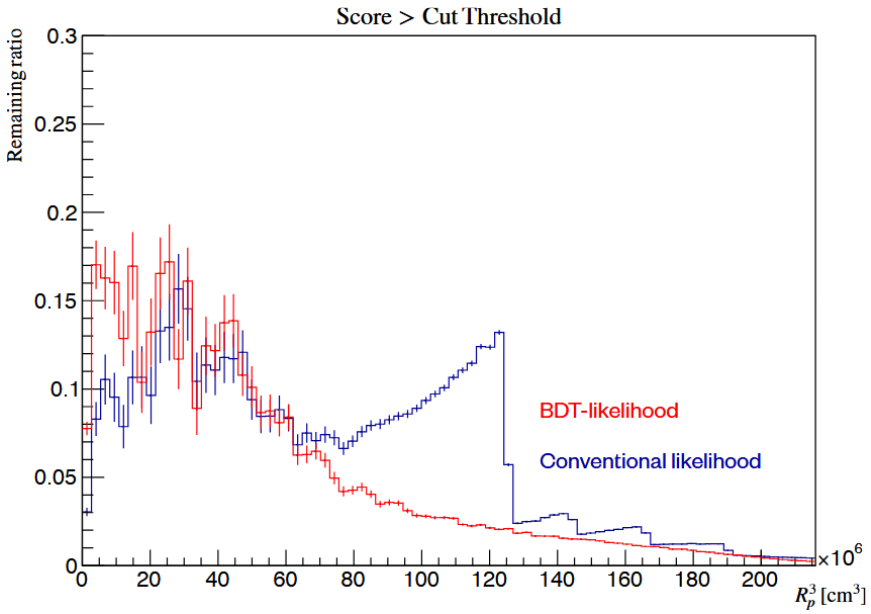

Distillation system in KamLAND site

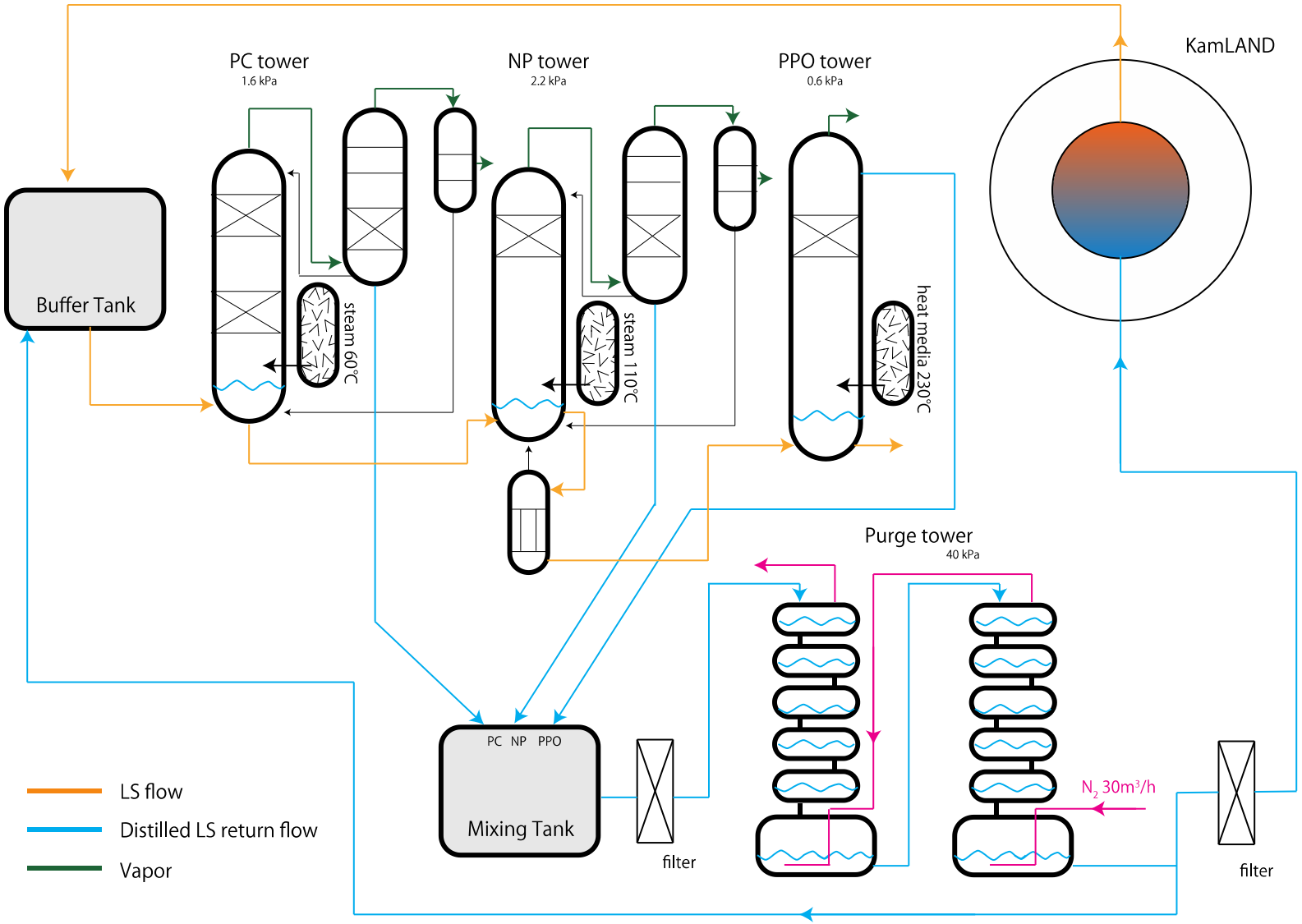

Neutrinoless double-beta decay

KamLAND's scientific program extends beyond neutrino observations. For example,,

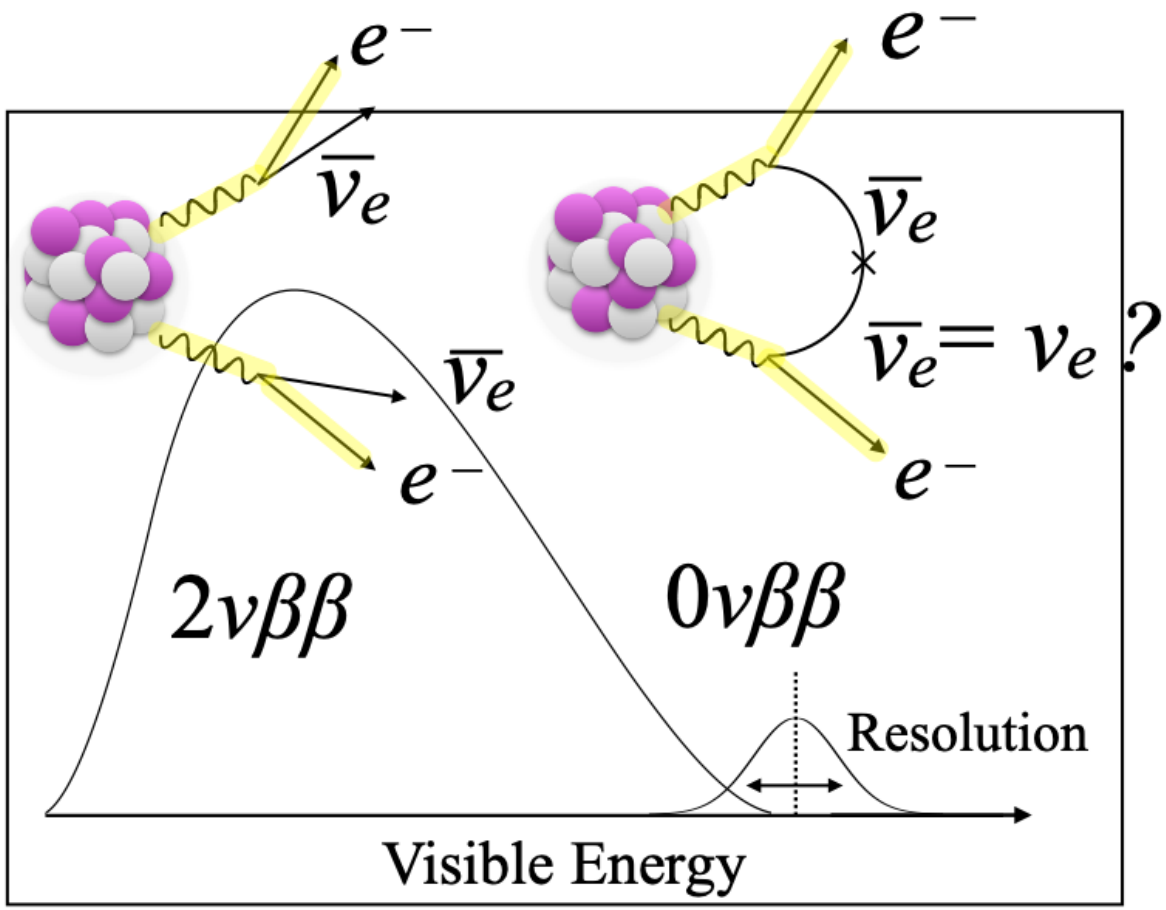

Majorana neutrino

- Neutrino can be Majorana particle.

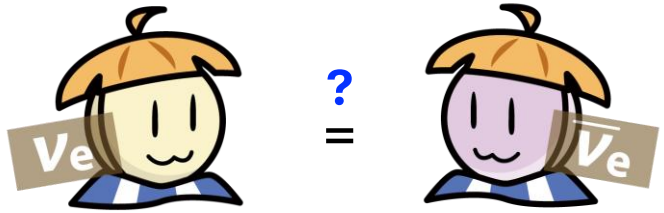

https://higgstan.com/

- Majorana neutrino is key componet of
  - Tiny neutrino mass (via SeeSaw mechanism)
  - Matter dominant universe (via Leptogenesis)

Neutrinoless double-beta decay (0νββ)

- It happens only if ν is Majorana particle.

Proof of Majorana neutrino

- Experiment: peak search around the Q-value
- Requirements: large exposure, background reduction

KamLAND is a suitable detector

KamLAND-Zen experiment

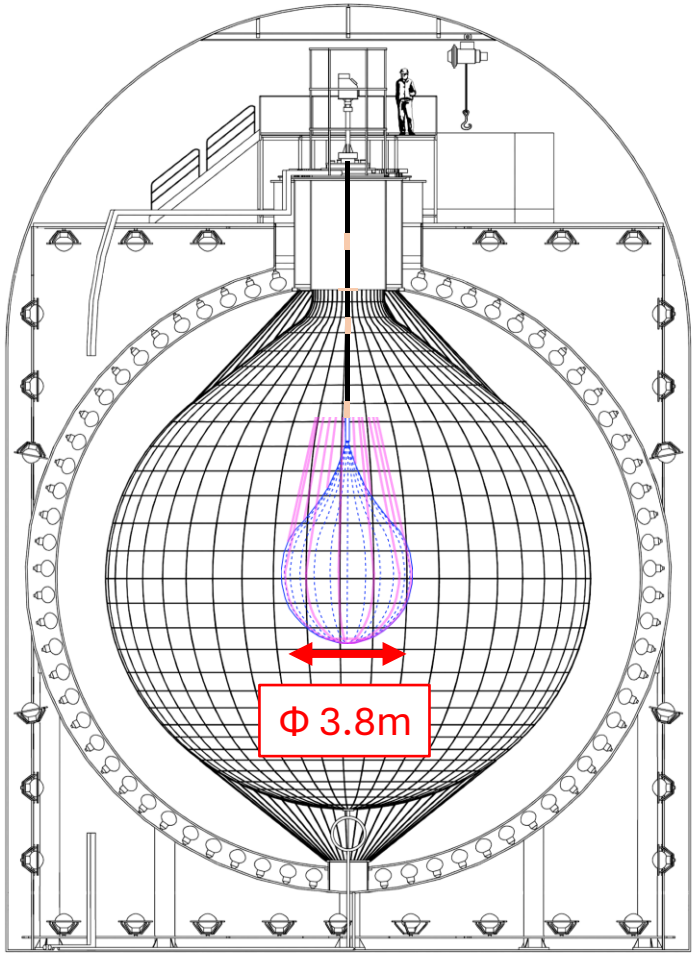

Zero-**n**eutrino double-beta decay search with **KamLAND** detector

Advantage of using the KamLAND detector

- Ultra-low radioactive environment – U, Th ≤ 10^{-17} g/g
- Huge & scalable – 1kt liquid scintillator

→ **Ideal enviromnet for extremely rare decay search !!**

Double-beta decay source : ^{136}Xe

- 0νββ Q-value : 2.46 MeV — below ^{208}Tl γ BG
- Long 2νββ half life — fewer 2νββ BG
- **(Relatively)** easy to enrich/purify by distillation — ^{136}Xe is enriched to ~90%
- Dissolved into liquid scintillator (LS) at 3%

Mini-balloon installed to support xenon-loaded LS (XeLS)

- Outer LS provides passive shielding from external radioactive background.
- Concentrated target nuclei can suppress volume-proportional backgrounds.

History and future of KamLAND-Zen

Past: 2011 – 2015

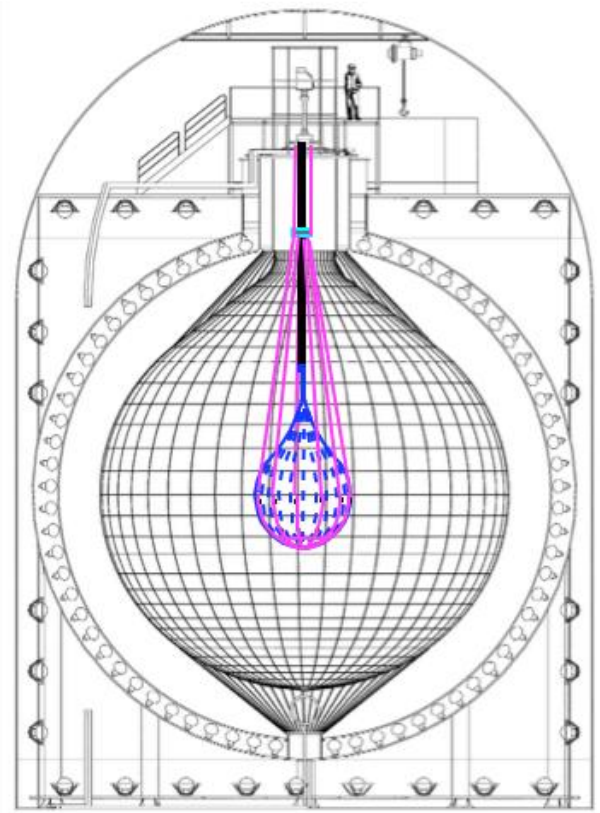

KamLAND-Zen 400

- Mini-balloon radius = 1.54 m
- 320–380 kg of enriched xenon
- $\langle m_{\beta\beta} \rangle < 61\text{–}165\ \mathrm{meV}$

Phys. Rev. Lett. 117, 082503 (2016)

Present: 2019 – 2024

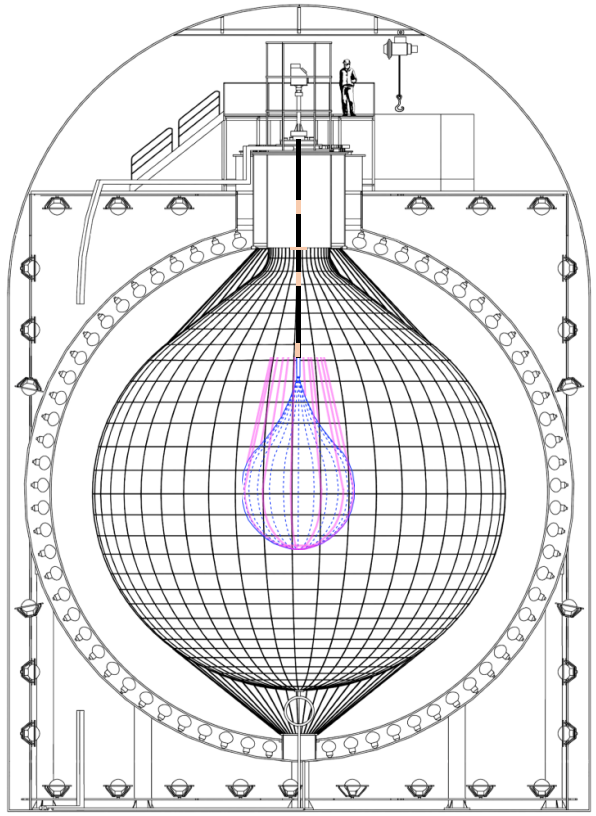

KamLAND-Zen 800

- Mini-balloon radius = 1.90 m
- 745±3 kg of enriched xenon

Cleaner mini-ballon, more xenon for better sensitivity

Phys. Rev. Lett. 130, 051801 (2023)

Under construction:

KamLAND2-Zen

- Detector upgrade for better energy resolution

Toward $\langle m_{\beta\beta} \rangle = 20\ \mathrm{meV}$ **!!**

KamLAND2(-Zen)

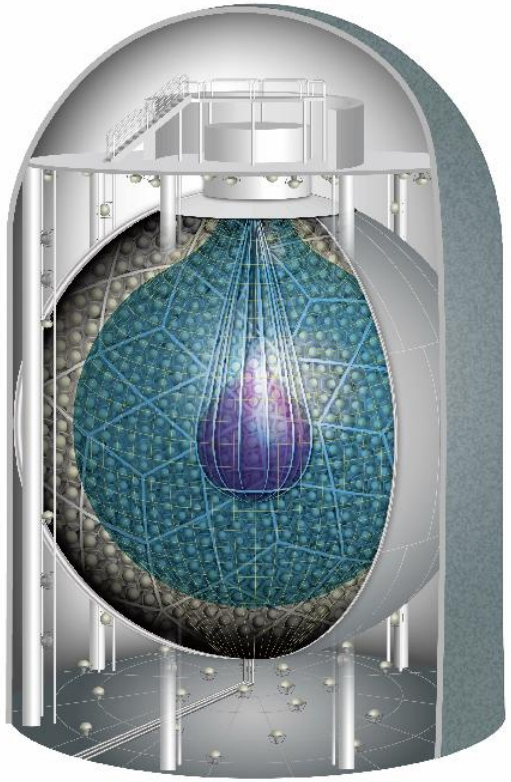

KamLAND2-Zen

Detector upgrade plan

- Light yield increase by
  - High light-yield scintillator (x1.4)
  - Light-correcting mirror on PMT (x1.8)
  - High quantum efficiency PMT (x1.9)

✓ x5 increased effective light yield
✓ Twice better energy resolution@Q-value
✓ 2νββ background reduction by order of 2.

- New mini-balloon of scintillating material

✓ Film-^{214}Bi rejection by α-tagging
✓ Expanding effective volume

- State-of-the-art read-out electronics: MoGURA2
  - RFSoC powered data acquisition
  - Huge buffer for SN-burst detection

✓ ~100% spallation neutron detection
✓ More efficient L.L. tagging

Target sensitivity

- The half-life : 2.0 × 10^{27} year
- $\langle m_{\beta\beta} \rangle \sim 20$ meV (in 10 years)
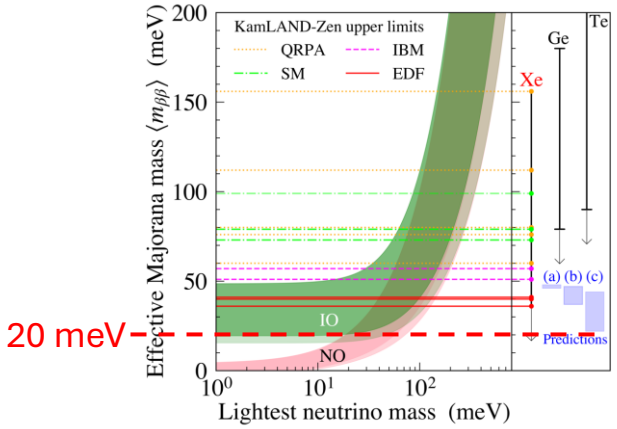
KamLAND2-Zen will be the first search to cover the Inverted-Ordering band !!